Development and validation of a high-resolution monthly gridded temperature and precipitation data set for Switzerland (1951–2000)

Dimitrios Gyalistras*

Climatology and Meteorology, Institute of Geography, University of Bern, Hallerstr. 12, 3012 Bern, Switzerland

ABSTRACT: A 5 km gridded temperature and precipitation data set was constructed for the topographically complex region of Switzerland in the European Alps. The data set consists of 1961–1990 mean fields for monthly mean temperature ($\overline{T}$) and monthly total precipitation ($\overline{P}$), plus monthly anomaly fields ΔT and ΔP for 1951–2000. All data are point estimates and come with extensive statistics on interpolation errors as a function of geographical location, elevation and time of the year. A novel interpolation method was employed that accounted for possible orographic effects at different spatial scales and allowed for regionally and seasonally varying relief-climate relationships. The accuracy of the interpolations was quantified by means of cross-validation. The proposed method was found to be superior to linear regression employing elevation as the only predictor for $\overline{P}$, and better than inverse distance weighting (IDW) interpolation for September to February ΔT. It was worse than IDW interpolation for springtime ΔT and for March to September ΔP. The areal mean cross-validation errors obtained for the new method were generally close to zero. The annually averaged mean absolute error for $\overline{T}$ was 0.6°C and for $\overline{P}$ it was 10.5 mm mo^{-1} (or 11%). The average proportion of temporal variance explained by the cross-validated monthly 1951–2000 station time series was 89% for ΔT and 81% for ΔP. The average proportion of spatial variance of the monthly anomaly fields explained was 13% for ΔT and 40% for ΔP. The largest cross-validation errors were generally found at regions of lower station density in south-southeast Switzerland and at elevations above ~2000 m above sea level. All error variances showed distinct annual cycles. The ΔT and ΔP fields and the derived trend fields showed substantial small-scale variability, which was not well reproduced and deserves further study. The individual gridpoint estimates should therefore be interpreted with care.

KEY WORDS: Interpolation · Complex terrain · Alps · Gridded data set · Temperature · Precipitation

1. INTRODUCTION

Information on the space-time variability of regional climate is important for basic climatological research and numerous applications, such as the validation of climate models, the construction of climate scenarios, or the study of climate change impacts and planning. In topographically and climatically complex regions such as Switzerland, the construction of appropriate, quantitative climatological data sets is particularly challenging. Switzerland lies in the central part of the European Alps, extends over an area of approximately 41 000 km^2, and covers an elevation range from ca. 200

to over 4500 m above sea level (masl). It is located at a latitude of 46 to 47.5° N, and at a distance of 600 to 800 km and a few hundreds of kilometers from the North Atlantic and Mediterranean coasts, respectively; thus its climate is shaped not only by a complex physiography but also by the interplay of oceanic, continental and subtropical climatic influences (Schüepp & Schirmer 1977, Schär et al. 1998, Wanner et al. 2000).

A generally applicable data set that would appropriately depict the large spatial, temporal and seasonal variability of the Swiss climate should fulfil several requirements: First, it should account for both radiative and thermal effects, as well as hydrological effects, by

considering at least the 2 primary variables, temperature and precipitation. Second, it should provide a high spatial and temporal resolution. A spatial resolution of a few kilometers or less is needed in order to resolve at least the major mountain ranges and valleys found in the study region; temporally, at least a monthly resolution is needed to capture the pronounced seasonality of the Swiss climate. Third, in order to account for the decadal-scale climate variability and any possible long-term trends, a suitable data set should extend over several decades. Fourth, in order to be universally applicable, and for ease of computerized data handling, the data set should cover the entire Swiss region and be defined on a regular grid. Fifth, the data set's accuracy should be well documented in order to enable users to estimate the reliability of any derived

results. Finally, the data set should be compared to any other similar data sets in order to offer potential users a basis for selection.

An impressive collection of digital, gridded climate data sets is already available for the Swiss region (Table 1). However, none of these data sets satisfies all the above requirements: several data sets consider only 1 variable at a time, e.g. only temperature or only precipitation; have an insufficient spatial extent (No. 9 in Table 1) or resolution (Nos. 2, 4, 5, 8, 10, 13, 14); do not account for the temporal variability of climate (Nos. 1, 2, 3, 5, 7, 11, 12); or cover periods of less than 30 yr (Nos. 4, 6, 11, 12). In most cases no detailed information is available on the quality and precision of the interpolated data sets over the Swiss region (exceptions are Nos. 7, 11 and 13). Moreover, only some of the

Table 1. Overview of gridded climate data sets for Switzerland. T: temperature; P: precipitation; *approximate longitude-latitude resolution of the grid in the vicinity of Switzerland; REP: regression using elevation as a predictor; IDW: inverse distance weighting; AURELHY: analysis using relief for hydrometeorological applications. ADW: angular distance weighting; GW: Gauss weighting; PRISM: parameter-elevation regression on independent slope model; RSOI: reduced space optimal interpolation; SYMAP: Synagraphic mapping system

No.	Variables	Spatial extent, grid resolution	Temporal extent, resolution	Number of stations, methods used	Source
1	T	Switzerland, 250 m	1931–1970, long-term	36, REP + IDW monthly means	Bär (1989)
2	T, P + cloudiness	Global land areas, 0.5° (38 km × 56 km)*	1930–1960, long-term monthly means	Several thousands, REP (T only) + thin-plate splines (Hutchinson & Bischof 1983)	Leemans & Cramer (1991)
3	P	Switzerland, 1 km	1951–1980, long-term monthly means	400 (corrected for gauge biases), REP + kriging	Kirchhofer & Sevruk (1992)
4	P	European Alps, 25 km	1971–1990, daily areal averages	6800, modified SYMAP (Shepard 1984, Willmott et al. 1985)	Frei & Schär (1998)
5	T, P + 7 other variables	Global land areas, 0.5° (38 km × 56 km)*	1961–1990, long-term monthly means	12 092 (T), 19 295 (P; Alps: ~320), trivariate thin-plate spline surfaces as a function of longitude, latitude and elevation (Hutchinson 1995)	New et al. (1999)
6	T, P + 3 other variables	Switzerland, 1 km	1973–1992, daily means	165 ($T + P$), REP (9 subregions, allowance for discontinuities in elevation profiles) + IDW (Schulla 1997)	Menzel (1999), Menzel et al. (1999)
7	P	Switzerland, 30″ (640 m × 920 m)*	1961–1994, long-term annual and seasonal means	306, AURELHY (Benichou & Le Breton 1987)	Neidhöfer (2000)
8	T, P + 5 other variables	Global land areas, 0.5° (38 km × 56 km)*	1901–1996, monthly mean anomalies	Several thousands (time varying network; Alps: 50–110), ADW	New et al. (2000)
9	T, P + 5 other variables	Switzerland, 1 km (10 605 forested locations only)	1969–1998, daily means	100 (T), 400 (P), REP (3 subregions, up to 2 discontinuities in T-elevation profiles) + IDW	Zierl (2000, 2001)
10	T	European Alps, 1° (76 km × 111 km)*	1760–1998, monthly mean anomalies	120 (time-varying network, homogenized), GW (2 elevation zones, no information transport across various subregions)	Böhm et al. (2001)
11	P	European Alps, 1.25″ (1.6 km × 2.3 km)	1971–1990, long-term annual and monthly means	6090, PRISM (Daly et al. 1994)	Schwarb (2001), Schwarb et al. (2001)
12	T + 8 other variables	Switzerland, 250 m	1971–1990, long-term monthly means for January, April, July and October	~70, REP (2 subregions) + kriging + empirical adjustments for the effects of aspect and cold-air ponds	Z'graggen (2001)
13	P	European Alps, 25 km	1901–1990, monthly mean anomalies	6800 (1971–1990), 140 (1901–1990), RSOI (Kaplan et al. 1997, Schmidli et al. 2001)	Schmidli et al. (2002)
14	T, P + 6 other variables	Global land areas, 10′ (13 km × 19 km)*	1961–1990, long-term monthly means	12 783 (T), 18 217 (P), same method as in New et al. (1999)	New et al. (2002)

studies cover the World Meteorological Organization standard period 1961–1990 (Nos. 5, 7, 8, 10, 13, 14), or appear to make good use of the abundant station data available for Switzerland (Nos. 3, 4, 7, 9, 11, 13). A few studies (Nos. 4, 7, 10, 11, 13) provide comparisons between selected data sets, but to my knowledge no systematic comparison of all the available data sets has been attempted so far.

In this paper I present the derivation and validation of a new 5 km × 5 km gridded monthly mean temperature and precipitation data set for Switzerland that covers the 50 yr period 1951–2000 and accounts for the complexity of the Alpine terrain. In order to meet the need of many applications for site-specific data (see e.g. Gyalistras et al. 1998), all interpolated gridpoint data present point estimates. The chosen resolution of 5 km is not as high as in some existing data sets (which provide a resolution of 1 km or less; Table 1), but it is still much higher than the ≥25 km resolution of all currently available long-term, time-dependent data sets (Nos. 8, 10 and 13). The monthly resolution is also coarser than the daily resolution of several existing data sets, but again, either these extend only over relatively short time periods (Nos. 6 and 9) or they were produced without taking into account the region's complex physiography (No. 4).

Several approaches can be envisaged for the development of a gridded climate data set. These include the interpolation of point or areal measurements with the aid of topographic-statistical techniques (see review in Section 2.2), simulations with physically based models (e.g. Barros & Lettenmaier 1994), or some combination of these approaches (e.g. Thompson et al. 1997, Purves & Hulton 2000). Simulation models have the advantage that they yield physically optimally consistent results. However, their application normally requires large amounts of input data for model initialization, forcing and testing. Moreover, the models also have huge computing requirements, which renders their use for the production of high-resolution, multi-decadal data sets impracticable.

Therefore, in the present work I focused on the statistical approach. This approach can in principle be applied to any combination of *in situ* and remote-sensed data (e.g. Vogt et al. 1997). However, the latter are available only for the last 20 to 30 yr, so the present study was based on *in situ* measurements only.

The production of the gridded data set was based on the 'anomaly' approach, as used by New et al. (1999, 2000). This approach builds upon the fact that monthly climate anomalies, which reflect the effects of large-scale circulation patterns, are spatially less variable and can thus be described by a less-extensive station network than the mean climate, which is more strongly tied to physiographic factors. Accordingly, below I

address the interpolation of (1) 1961–1990 monthly long-term mean fields based on an extensive climate station network; and (2) monthly anomaly fields for all months in 1951–2000 based on a reduced set of long-term stations.

Most of the studies listed in Table 1 either did not account for the influence of the relief or did so only in a relatively simple manner. Exceptions are the works by Neidhöfer (2000) and Schwarb (2001). Both authors used sophisticated topographic-statistical methods to interpolate long-term mean climate, which will be discussed later in more detail.

To my knowledge, such sophisticated methods have not been applied to interpolate temporally varying fields in the Swiss region until now. In particular, New et al. (2000), Böhm et al. (2001) and Schmidli et al. (2002) constructed anomaly fields that did not account for any possible orographic effects. This approach appears justifiable in view of the relatively sparse station networks and coarse spatial resolutions (≥25 km) considered in these studies. However, it may be expected that with increasing spatial or temporal resolution the role of relief becomes progressively more important.

In the present work I investigate how relief information can be used to improve not only the interpolation of long-term mean fields, but also that of 5 km anomaly fields. The interpolation procedure employed was based on the method proposed by Benichou & Le Breton (1987), which I extended in order to account for orographic variability at different spatial scales, as well as for regionally and seasonally varying relief-climate relationships. The amount and detail of orographic information that entered the interpolations were adjusted as a function of variable and station-network density.

It is shown, firstly, that the newly proposed method clearly improves the interpolation of long-term mean precipitation and of autumn and winter temperature anomalies compared with simpler methods. However, with regard to spring or summer climate anomalies, better results can be obtained from a simpler procedure. Secondly, it is found that the quality of the interpolations shows distinct regional and seasonal patterns that are quite independent of the interpolation method employed and have plausible climatological explanations. Finally, this work demonstrates that local climate trends, in particular local temperature trends, may show surprisingly high small-scale variability, which cannot be easily captured by interpolation.

Section 2 describes the data and methods used to produce, test and analyze the gridded data sets. In Sections 3 and 4, the results are presented and discussed. These include a brief 50 yr trend analysis of the Swiss temperature and precipitation fields. The paper ends with conclusions on the proposed interpolation method and the accuracy and utility of the new data set (Section 5).

2. DATA AND METHODS

2.1. Data. Two kinds of data were used: point elevation data from 2 digital elevation models (DEM), covering the European and Swiss regions, respectively; and monthly temperature and precipitation station data from a large number of Swiss climate stations.

2.1.1. Elevation data: The European-scale DEM data were downloaded from the Webpage of 'The Global Land One-km Base Elevation Project' (GLOBE; Hastings & Dunbar 1998; http://www.ngdc.noaa.gov/seg/topo/globe.shtml, accessed on April 9, 2002). This DEM has a resolution of 30 arc-sec, which in the Swiss area corresponds to a longitude × latitude resolution of 640 m × 920 m. The root-mean-square error (RMSE) of GLOBE over Europe should generally be below 20 m (Hastings & Dunbar 1998). Comparison of the GLOBE-DEM with the Swiss DHM25-DEM (see below) showed a mean error over the Swiss region of –4 m and a RMSE of ~150 m. About 10% of the ~53 000 data points compared showed differences greater than 250 m.

The Swiss DEM was the 'Digitales Höhenmodell' of the Swiss Federal Office of Topography (DHM25, quality level 1; Landestopographie 2001a), which has a resolution of 25 m. The average error of the DHM25-DEM in northern Switzerland (Swiss Plateau and Jura mountains) is 1.5 m, in the Swiss Prealps and southern Switzerland (Tessin) 2 m, and in the Alps 3 m.

For the present study I derived a new 1 km × 1 km longitude-latitude DEM by merging the 2 data sets as follows: First, every 40th point from the DHM25-DEM was sampled to obtain a 1 km grid (one-fifth of the resolution of the 5 km target grid). Second, the GLOBE-DEM was regridded to match the Swiss km coordinate system (Landestopographie 2001b), again using a gridpoint distance of 1 km. Regridding was done by fitting a partial quartic equation to the 9 closest gridpoints of the original data set. The equation is such that the resulting surface passes exactly through the 9 gridpoint elevations (Zevenbergen & Thorne 1987). Finally, the 2 data sets were merged by using, wherever possible, the data from DHM25.

The newly produced DEM was named DEM-A. It is optimally precise within Switzerland at a 1 km resolution and less precise in the surrounding regions. Two further DEMs with coarser resolution, which were named DEM-B and DEM-C, were derived (1) by taking spatial averages from DEM-A using sliding windows of 3 km × 3 km and 5 km × 5 km, and (2) by sampling every third and fifth gridpoint, respectively, from the smoothed data sets.

2.1.2. Climatic data: Time series of monthly mean daily mean temperatures (T) and of monthly precipitation totals (P) were extracted for the years 1901–2000 from the database of the Swiss Meteorological Institute. Data prior to 1951 were extracted to calibrate regression models that were used for the estimation of missing values in 1951–2000 (see below). Homogenized time series were used where available (Aschwanden et al. 1996).

No further tests for data quality or homogeneity were performed. Rather than performing the very costly task of identifying and removing any inhomogeneities prior to carrying out the interpolations, the present study aimed at quantifying the inhomogeneities' possible effects with the aid of cross-validation. In cross-validation, 1 data point is excluded at a time, and it is then predicted from all the remaining data (see also Section 2.3). The reasoning was as follows: the prediction of an inhomogeneous data point at a given location from the surrounding, homogeneous station data should automatically lead to a relatively large cross-validation error for that particular point; conversely, the use of that data point to predict all others would be likely to distort the empirical climate-relief relationship, thus increasing the cross-validation error at the surrounding locations. Hence, any inhomogeneities should become documented implicitly in the form of increased cross-validation errors. This issue is discussed further in Section 4.2.

The SMI database contained data for 191 *T* stations and 673 *P* stations, but only 56 and 313 stations, respectively, fully covered 1961–1990. Therefore linear regressions from neighboring climate stations were used to predict missing station values and to generate an extended data set. This simple approach appeared justified because correlations between neighboring stations were generally found to be very high (see below). A square-root transformation was applied to all *P* data prior to fitting the regressions, because *P* was found to be positively skewed for most locations and months.

The 'best' neighbor station to estimate a missing monthly value was determined according to the following algorithm:

• Step 1: Find for the given target variable and month all stations with at least 20 years of data in 1901–2000.

• Step 2: Determine all stations that have at least 20 yr of common data with the target station.

• Step 3: Compute the linear regressions between the target station and all these stations.

• Step 4: Select all stations for which the coefficient of determination (r^2) is larger than 0.5. (This value was well above the threshold r^2 value of ~0.2 that indicates a correlation different from zero at the 95% significance level [n = 20].)

• Step 5: If at least 1 such station exists, use for interpolation the station with the largest r^2; otherwise retain the missing value at the target station.

Thanks to the availability of a dense original station network, the average r^2 values of the regressions amounted to 96% for T and 92% for the square-root transform of P. The procedure resulted in a new network of 136 T stations and 515 P stations that fully covered 1961–1990. The average distance between a station and its closest neighbor (its closest 50 neighbors) was 9.6 (61) km for T and 5.1 (27) km for P.

Two further networks of climate stations resulted by selecting from the SMI database all stations with at least 45 yr of data available in 1951–2000. These were 35 stations for T and 147 stations for P. Here no time interpolation of missing values was done. The average distance between a station and its closest neighbor (its closest 25 neighbors) amounted to 24 (95) km for T and 10.5 (37) km for P.

The climate stations' distribution with elevation is shown in Fig. 1. It can be seen that for all 4 station networks only very few stations were available below 250 and above 2000 masl. The fraction of the Swiss area that falls in the elevation zones 0–250, 250–1500, 1500–2000, 2000–2500 and ≥2500 masl is 1, 63, 13, 13 and 10%, respectively. The higher elevation regions were therefore underrepresented in all station networks.

For all stations of the 2 extensive networks, the 1961–1990 monthly long-term mean values ($\overline{T}$ and $\overline{P}$) were computed as an input for the interpolation of the long-term mean fields. Monthly departures ΔT and ΔP from the 1961–1990 means were computed for the 2 other networks and 1951–2000. They provided the input for the interpolation of the monthly anomaly fields.

2.2. Interpolation method. The interpolation method consisted of the following steps, which are typical for most topographic-statistical interpolation studies: (1) description of the relief by means of a set of predictor variables; (2) evaluation of these variables at the climate station locations and at all target grid-points; (3) establishment of a statistical model at the climate stations to estimate the quantity of interest from the orographic predictors; (4) application of this model to the entire target grid.

The following subsections address the choice and implementation of the particular approach used in the present study.

2.2.1. Choice of topographic predictors and interpolation method: Topography (vegetation, land use, inland bodies of water, relief, etc.) influences the cli-
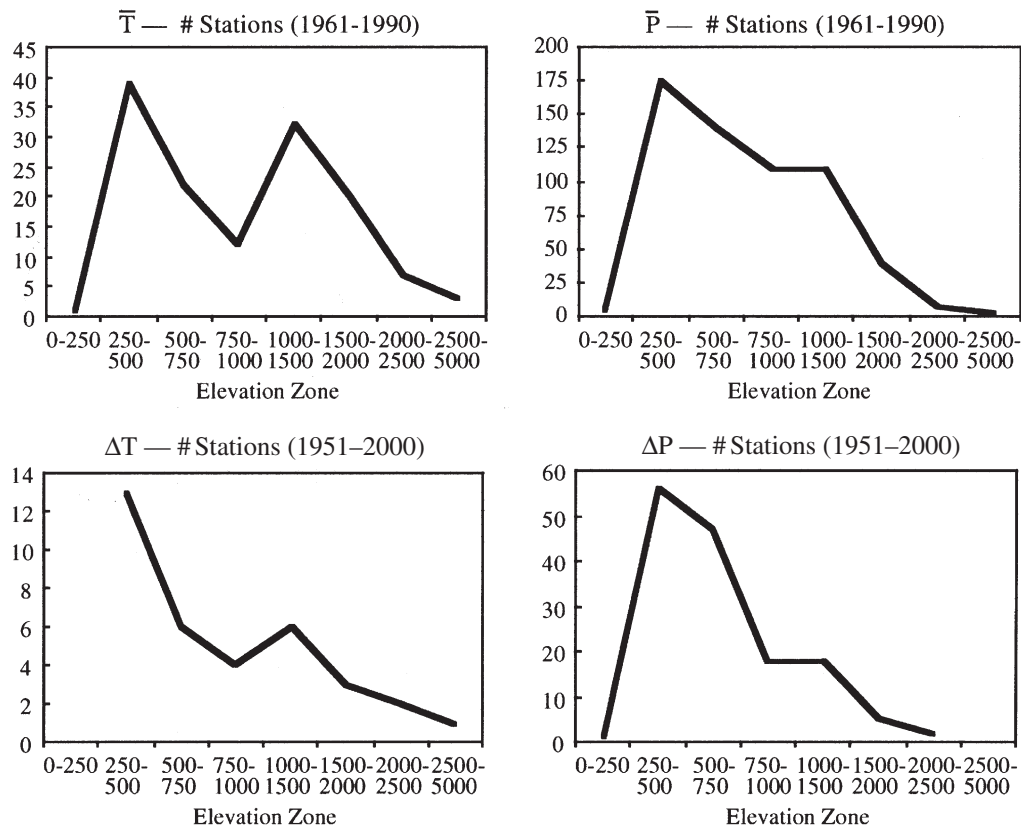
Fig. 1. Numbers of climate stations that were available for interpolation as a function of station elevation (masl). $\overline{T}$: long-term mean monthly mean temperature; $\overline{P}$: long-term mean monthly total precipitation; ΔT: monthly mean temperature anomaly; ΔP: monthly precipitation anomaly

mate in many ways, and there are no universal rules to guide the choice of topographic predictor variables. Longitude and latitude have been used in several studies in order to account for general spatial trends, for instance, due to systematic variations in insolation or due to the presence of large bodies of water or mountains (e.g. Holdaway 1996, Kurtzman & Kadmon 1999). Detailed descriptions of the relief can be obtained from a DEM. Frequently used variables are point elevation (e.g. Phillips et al. 1992, Dodson & Marks 1997), slope and aspect, and the distance from large upwind orographic barriers (e.g. Basist et al. 1994, Carrega 1995). All these variables can also be evaluated as a function of direction (e.g. Prudhomme & Reed 1998, Agnew & Palutikof 2000).

In most topographic-statistical methods the topographic predictors and the target variable are linked to each other by means of multiple linear regression. In complex terrain it is appropriate to account for local and regional changes in topographic regime, for instance, by using regionally, or even continuously, varying relief-climate relationships. This can be done based on a windowing (Daly et al. 1994, Schwarb 2001) or distance weighting (Brunsdon et al. 2001) technique. Moreover, it may be appropriate to use seasonally varying regression equations in order to account for temporally varying lapse rates, prevailing wind directions, etc. (e.g. Pepin 2001).

Since in Switzerland no single factor (such as elevation) can be expected to determine the distribution of climatic elements, it was decided to use a procedure that allows for inclusion of sophisticated orographic information. The following 3 candidate methods were identified based on a literature review:

(1) AURELHY (analysis using relief for hydrometeorological applications; Benichou & Le Breton 1987). A principal component analysis (PCA, e.g. Preisendorfer 1988) is applied to a large number of elevation vectors that represent small areas (e.g. 11×11 DEM gridpoints), which are sampled from the study domain. The principal component (PC) loadings of the first few PCs provide a description of the most important patterns of orographic variability at a scale comparable to the size of the small areas used for PCA. The PC scores are used as orographic predictors. This method was used by Neidhöfer (2000) to interpolate long-term mean annual and seasonal precipitation fields for Switzerland. His work is discussed later in more detail.

(2) PRISM (parameter-elevation regression on independent slope model; Daly et al. 1994). The relief is described based on DEM-derived areal mean elevation and on the definition of so-called 'facets', i.e. contiguous areas of more-or-less constant slope orientation at different DEM resolutions. Schwarb (2001) successfully applied the PRISM method to produce

maps of long-term mean annual and monthly precipitation in the European Alps at a ~2 km resolution.

(3) PLUVIA (Drogue et al. 2002). The relief in the vicinity of a given target location is described based on a whole range of elevation statistics of neighboring DEM gridpoints, such as the mean, standard deviation and various quantiles. The statistics are evaluated separately for 8 directions and for square areas of 1×1 to 29×29 km^2. To my knowledge this method has not been applied in the Swiss region until now.

I decided to use the AURELHY method because it provides an efficient and elegant representation of the relief; it uses orthogonal predictors (the PC scores) as inputs for the statistical prediction; and it requires adjustment of only a relatively small number of parameters, which are mainly related to the set-up of the PCA. Quite differently, the use of the PRISM method would have required considerable time for tuning of at least 16 parameters related to the definition of the facets and the selection of appropriate neighboring stations and their weights for fitting of the regression equations (Schwarb 2001). This also made PRISM appear less suitable for the automated interpolation of a larger number of monthly, time-varying fields. The PLUVIA method could have been a somewhat better choice for the interpolation of precipitation fields than the original AURELHY method (see comparison by Humbert et al. 1997), but it was not used because it does not account for slope aspect, which was assumed to be important for the interpolation of the temperature fields.

2.2.2. Extensions of the AURELHY method: Two main disadvantages of the original AURELHY method are (1) that it considers only a single scale of orographic variablity, as defined by the size and geometry of the small areas used for PCA and (2) that it assumes a constant relief-predictand relationship throughout the entire domain. I therefore attempted to improve the method as described below.

The first problem was analyzed in detail by Neidhöfer (2000). He found that the quality of the orographic regression models used to predict precipitation depended sensitively on the definition (area size and sampling region) of the elevation vectors used for PCA, and that the optimal definitions varied strongly with season and region. In order to alleviate this problem I subdivided the Swiss region into small subsectors of 50 km × 50 km (Fig. 2) and to compute, for each of the 40 subsectors, 3 different PCAs (PCA-A to -C) that focused on 3 different space scales (Table 2).

With regard to the second problem, Neidhöfer (2000) defined 7 subregions and used regionally varying regressions. However, he found large discontinuities of the interpolated precipitation fields at the subregion's boundaries, and this suggested that his approach did not capture the spatial variability of the relief-precipitation
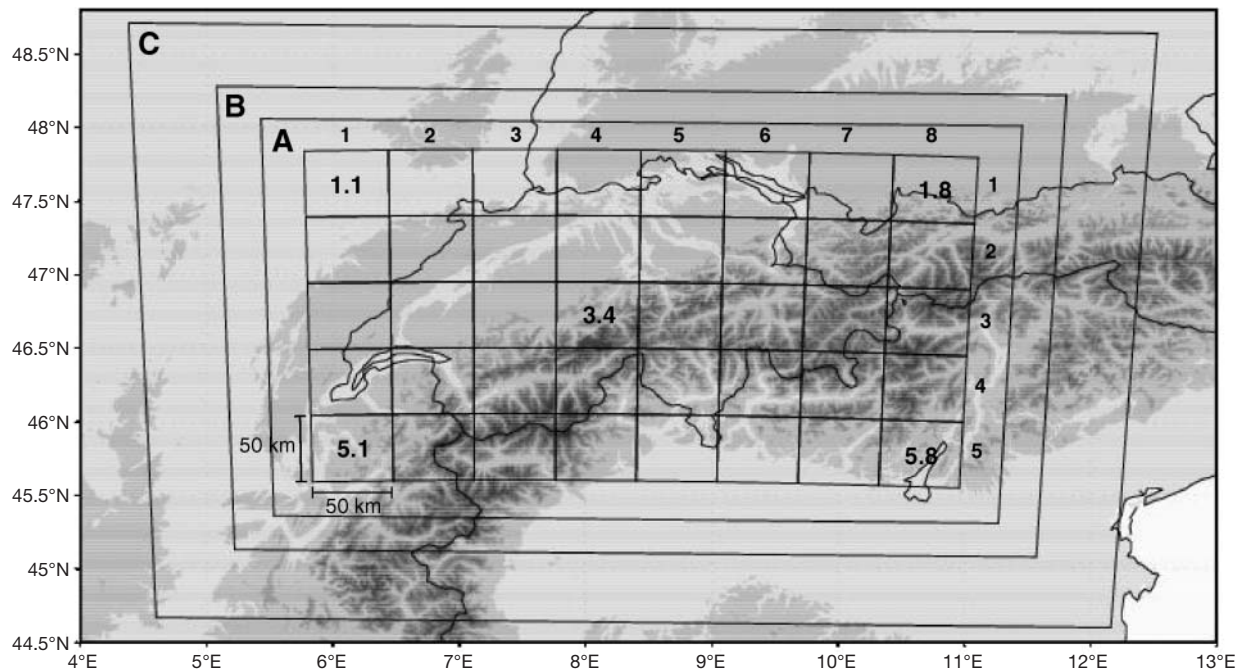
Fig. 2. Elevation map of the study domain and definition of the different sectors used in the interpolation procedure. A, B, C: sectors covered by the digital elevation model (DEM) data sets used; A: sector containing point elevation data; B, C: sectors containing elevation data averaged over quadratic areas of size 3×3 km and 5×5 km, respectively; 1–5 and 1–8: row and column numbers used to denote subsectors; 3.4: example for a selected subsector. For each subsector 3 different principal component analyses (PCAs) for the 3 elevation data sets A–C were performed using data from surrounding areas of size 100×100 km (A), 150×150 km (B), and 250×250 km (C)

relationship well enough. Therefore, in the present study I used site-specific regression equations, which were determined separately for every single target gridpoint of every interpolated long-term mean or anomaly field. This approach was adopted again for both temperature and precipitation.

The choice of using 3 PCAs per Swiss subsector in the present study was to some extent arbitrary. It presented a compromise between the conflicting needs to accurately describe relief variability over a sufficiently wide range of spatial scales, on the one hand, and on the other hand, to keep the total number of orographic predictors small compared to the maximum number of 25 to 50 stations that were used to fit the orographic regressions (Table 3).

The sizes (S^2) of the quadratic areas used to compute the 3 PCAs were chosen based on the following considerations: Initial experimentation with dif-

Table 2. Characterization of the digital elevation models (DEM) used, and of the principal component analyses (PCA) applied to the 3 DEM data sets in the surroundings of every Swiss subsector (see Fig. 2)

	DEM-A	DEM-B	DEM-C
Spatial resolution (km; longitude × latitude)	1×1	3×3	5×5
Meaning of gridpoint data	Point elevation, merged from the 'DHM25' and 'GLOBE' DEMs	Average of 3×3 gridpoints from DEM-A	Average of 5×5 gridpoints from DEM-A
	PCA-A	PCA-B	PCA-C
Size of area used to sample elevation vectors for PCA (km; longitude × latitude)	100×100	150×150	250×250
Size of area represented by each elevation vector used for PCA (S^2, km; longitude × latitude)	11×11	63×63	125×125
Sampling interval for elevation vectors used for PCA (km; longitude/latitude)	5/5	6/6	10/10
Number of elements per elevation vector used for PCA	$11^2 = 121$	$21^2 = 441$	$25^2 = 625$
Number of elevation vectors used for PCA	$19^2 = 361$	$16^2 = 256$	$14^2 = 196$

Table 3. Parameters of the interpolation procedure. $\overline{T}$: long-term mean monthly mean temperature; ΔT: monthly mean temperature anomaly; $\overline{P}$: long-term mean monthly total precipitation; ΔP: monthly precipitation anomaly. PC: principal component; PCA: principal component analysis

	$\overline{T}$	ΔT	$\overline{P}$	ΔP
Use point elevation/ Use areal mean elevation	Yes/Yes	Yes/Yes	Yes/Yes	Yes/Yes
Number of PCs from PCA-A/PCA-B/PCA-C (N_{PCA-X})	3/3/3	0/1/1	3/3/3	0/2/2
Maximum number of climate stations	50	25	50	50
Maximum radius of influence of climate stations (R; km)	100	150	50	75

ferent PCAs showed that the loadings of the first and second PCs corresponded in most cases either to an inclined surface or to a single trough or ridge (Fig. 3a,b). For the third PC loadings, a saddle point was typically obtained, or a combination of a single trough and a ridge, i.e. an oscillating pattern with wavelength $\geq S$ (not shown). Hence the scale of orographic variability resolved by the first 2 and 3 PCs was found to be ~S and $\geq S/2$, respectively. In order to ensure that a station network matches this resolution, it was concluded that $S \geq \kappa \overline{D}_s$, with κ ranging between 1 and 2, and $\overline{D}_s$ is the average distance between neighboring stations (i.e. each station sampled an area of average size $\overline{D}_s$).

This led to the following choices for S: For $\overline{T}$ and $\overline{P}$, $\overline{D}_s$ = 9.6 and 5.1 km, respectively, such that for PCA-A, S = 11 km. For ΔT and ΔP, $\overline{D}_s$ = 24 and 10.5 km. However, the individual distances between neighboring stations in the 2 anomaly networks varied considerably, between 6.2 and 68 km for ΔT, and between 2.3 and 38 km for ΔP. Therefore, for PCA-B, S = 63 km. Whereas PCA-A and PCA-B accounted for the small- and mesoscale variability of the relief, a further PCA, PCA-C, was used to account for climate variations due to large-scale topographic forcing: S = 125 km.

As an example, results of the 3 PCA analyses for the subsector 3.4 (Fig. 2) are shown in Fig. 3. The first PC loading of PCA-A described variations in the aspect (northwest for positive and southeast for negative PC scores; Fig. 3a), whereas the loading of the second PC provided a measure of the terrain curvature in the surroundings of a location (trough-like relief for positive and ridge-like relief for negative PC scores; Fig. 3b). The first PC loading maps from both PCA-B and PCA-C again provided a measure of aspect, but on progressively larger spatial scales (Fig. 3a). The second arc-shaped PC loadings accounted for the position of a target location relative to the entire Alpine range (Fig. 3b). Similar results were obtained for the other subsectors, but the orientation, shape and order of the patterns varied considerably between subsectors (not shown).

2.2.3. Set-up of the interpolation procedure:
The predictors used to fit the orographic regressions were: (1) point elevation; (2) areal mean elevation; and (3) a varying number of PC scores from PCA-A to -C (Table 3). These variables were computed as follows:

For fitting of the regression models the point elevations ($h_{(x,y)}$, where x and y denote the space coordinates) were given by the station elevations; for model application at the station locations or the target gridpoints they were determined from DEM-A. Areal mean elevation ($g_{(x,y)}$) was determined at a 1 km resolution by applying a 5 km × 5 km sliding window to DEM-A. The PC scores ($s_{Xi(x,y)}$, X = A–C, i = 1 … N_{PCA-X}; see Table 3) for a given target gridpoint were obtained by projecting the respective PC loadings map ($\vec{p}_{X_i}$) onto an elevation anomaly vector ($\vec{a}_{X(x,y)}$), which was derived from an elevation vector ($\vec{h}_{X(x,y)}$) that was centered over the target location (x,y). The anomalies were taken relative to the mean ($\vec{m}_X$) of all elevation vectors used to perform the respective PCA (Table 2):

$$s_{X_i(x,y)} \;=\; \vec{a}^{\,T}_{X(x,y)} \cdot \vec{p}_{X_i} = (\vec{H}_{X(x,y)} - \vec{m}_X)^T \cdot \vec{p}_{X_i} \qquad (1)$$

(The superscript T denotes the transpose of a vector.) The predictor variables at the climate station locations (which normally did not coincide with a gridpoint of the target grid) were estimated with the aid of a partial quartic equation (Zevenbergen & Thorne 1987) using the 9 closest gridpoints from the respective DEM or gridded PC scores data set.

The spatial distributions of selected PC scores $s_{Xi(x,y)}$ for subsector 3.4 are shown in Fig. 3c,d.

The quantity of interest at a given target location (x,y) was estimated according to:

$$\hat{F}_{(x,y)} \;=\; a + b \cdot h_{(x,y)} + c \cdot g_{(x,y)} + \sum_X \sum_{i=1}^{N_{PCA-X}} d_{X_i} \cdot s_{X_i(x,y)} \qquad (2)$$

Here the ^ denotes an estimate, and $F = \overline{T}$, $\overline{P}$, $\Delta T(t)$ or $\Delta P(t)$, where t denotes time; a, b, c and d_{X_i} are site-specific (and in the case of the anomaly fields also time-varying) regression parameters that were estimated using data from the climate stations surrounding the target location (see below); and the summation over X depended on the variable considered (Table 3).

Note that the present study considered only a possible orographic signal, i.e. no interpolation of the residuals from the regression according to Eq. (2) was employed. The only post-processing consisted in limiting all interpolated precipitation values to ≥ 0.

The first 3 PCs from each PCA were always used for the interpolation of $\overline{T}$ and $\overline{P}$. This number was deter-
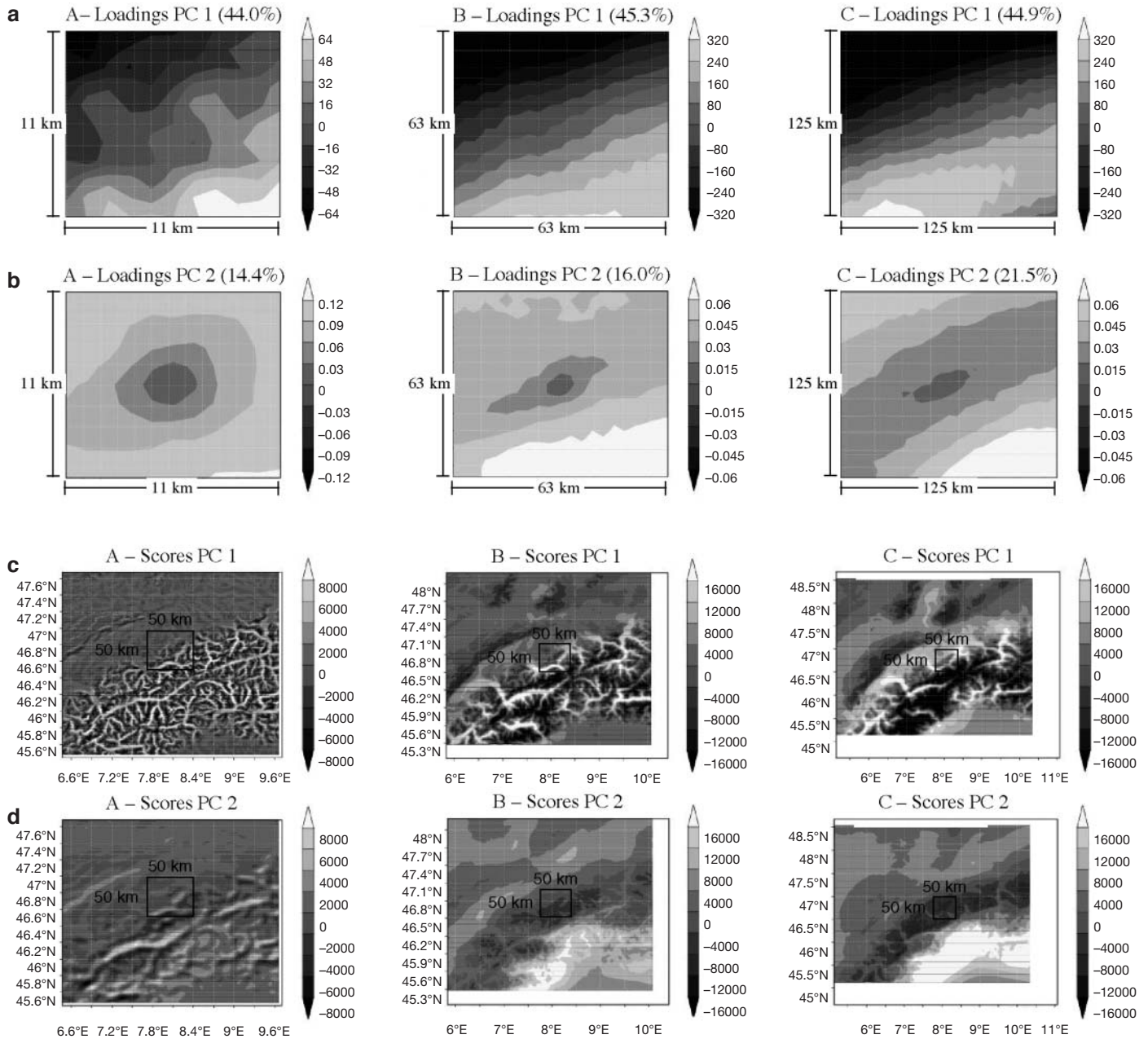
Fig. 3. Results of the 3 principal component analyses (PCA-A to -C) for subsector 3.4 (see Fig. 2 and the 50×50 km boxes in panels c and d. (a,b) Loadings maps of the first and second PCs, respectively; (c,d) scores of the first and second PCs. Loadings are given in m; scores are arbitrary units. Percentages in (a) and (b) give the proportions of the total variance explained by each PC

mined by inspecting the eigenvalue spectra of the various PCAs, which in most cases levelled off after the third PC. The first 3 PCs typically explained up to 95% of the total variance of the elevation data set used for PCA. Smaller numbers of PCs were used for the interpolation of ΔT and ΔP, and only those from PCA-B and PCA-C, in order to account for the less-extensive station networks.

The data for the fitting of the linear regressions at a given target location were taken either from all stations found within a given radius of influence (R) around this location or from a maximum number of sta-

tions found at a distance $\leq R$, whichever criterion was satisfied first (Table 3). All stations found were considered in the regression with the same weight.

The value of R used for the interpolation of $(\overline{P})$ was set to 50 km. Schwarb (2001) found that the semi-variogram of annual mean $\overline{P}$ from 6000 Alpine stations can be described by an exponential function with a range of 1.3° (approx. 100 to 150 km). In the present study a smaller value was used in order to account for the higher spatial variability of the monthly $\overline{P}$ fields. For the interpolation of $\overline{T}$, which after detrending

for elevation showed a smoother behavior than $\overline{P}$, $R = 100$ km was used (Table 3).

In order to determine R for the interpolation of ΔT and ΔP, the variances (V, in %) that are explained by simple linear regression between 2 stations were investigated as a function of distance (D, in km). For annual mean ΔT and the distance range 0–250 km, $V = 89 - 0.07D$. Hence, stations up to a distance of several hundred kilometers from a target location could have been used. However, I chose $R = 150$ km for all months, because a much stronger decay of correlation with distance was found for October to December, when regional temperature inversions occur quite frequently in some valleys and parts of the Swiss Plateau. For annual mean ΔP and the distance range 0–150 km, $V = 72 - 0.29D$. Stronger decreases in correlation with distance were found for April to July, probably due to the more frequent occurrence of convective conditions during these months. However, for the sake of simplicity, $R = 75$ km was always used, i.e. the distance at which V dropped to 50 % for annual mean ΔP.

2.3. Alternative interpolation methods. For $\overline{T}$ and $\overline{P}$ the newly proposed interpolation method was compared to a much simpler method, which used only local elevation as a predictor (REP in Table 1). The corresponding regression model was given by the first 2 terms on the right-hand side of Eq. (2).

With regard to ΔT and ΔP, an inverse distance weighting (IDW) procedure was considered. IDW does not account for any orographic effects and computes the target quantity as a weighted mean of the measured values at the surrounding stations. The weights used for each station are proportional to $(1/d)^\alpha$, where d is the station's distance from the target location. Values of 0.5 (i.e. distant stations receive a relatively large weight), 1.0, and 2.0 (rapid decay of a station's influence with distance) were considered for the parameter α.

The climate stations used by the 2 alternative procedures were selected in the same manner as reported in Table 3.

2.4. Validation. The performance of all interpolation procedures was assessed by means of cross-validation, which was performed for every single interpolated monthly long-term mean or anomaly field as follows: each climate station was excluded once from the given station network, and the target quantity of interest was then predicted at this station using the data from all remaining stations. The predicted and measured values were compared using a series of statistics that are summarized in Table 4.

Note that the ME, MAE, MRE and MARE statistics (Table 4) gave the same weight to all errors, whereas the RMSE and RMSRE statistics gave higher weight to larger errors compared to smaller ones. Note also that COR and PEV do not carry physical dimensions. They

were used to measure the pattern similarity between the interpolated and observed data fields.

COR varies between +1 and –1 and does not account for any systematic errors in the mean or the variance. It measures the degree to which a linear transformation of the interpolated data could be used to reproduce the measurements, with values of ±1 indicating the possibility of a perfect fit.

The PEV statistic assumes values between $-\infty$ and +1. Values <0 indicate very poor performance of the interpolation procedure; a value of zero suggests that the interpolation is no better than using the mean; and values > 0 suggest a useful result in the sense that the error vari-

Table 4. Statistics used to analyze the station data and to assess the accuracy of the interpolations. x_i: ith measured value; y_i: ith predicted value from the cross-validation procedure; N: number of samples considered; $\overline{x}$: mean of all measured values; $\overline{y}$: mean of all predicted values

Statistic	Identifier	Definition
Mean	MEAN	$\frac{1}{N}\sum x_i$
Standard deviation	SD	$\sqrt{\frac{1}{N-1}\sum(x_i - \overline{x})^2}$
Mean absolute deviation	MAD	$\frac{1}{N}\sum|x_i - \overline{x}|$
Trend	TREND	Slope of linear regression from time
Error	E	$y_i - x_i$
Absolute error	AE	$|y_i - x_i|$
Relative error	RE	$\dfrac{y_i - x_i}{x_i}$
Absolute relative error	ARE	$\left|\dfrac{y_i - x_i}{x_i}\right|$
Mean error	ME	$\frac{1}{N}\sum(y_i - x_i)$
Mean absolute error	MAE	$\frac{1}{N}\sum|y_i - x_i|$
Root-mean-square error	RMSE	$\sqrt{\frac{1}{N}\sum(y_i - x_i)^2}$
Mean relative error	MRE	$\frac{1}{N}\sum\dfrac{y_i - x_i}{x_i}$
Mean absolute relative error	MARE	$\frac{1}{N}\sum\left|\dfrac{y_i - x_i}{x_i}\right|$
Root-mean-square relative error	RMSRE	$\sqrt{\frac{1}{N}\sum\left(\dfrac{y_i - x_i}{x_i}\right)^2}$
Correlation coefficient	COR	$\dfrac{\sum(y_i - \overline{y})(x_i - \overline{x})}{\sqrt{\sum(y_i - \overline{y})^2}\sqrt{\sum(x_i - \overline{x})^2}}$
Proportion of explained variance	PEV	$1 - \left(\sum(y_i - x_i)^2 \big/ \sum(x_i - \overline{x})^2\right)$

ance is smaller than the variance of the original data set.

The various statistics were evaluated either for all climate stations (or all stations within a given elevation zone) or across all time points. Hereafter the kind of summation used to derive a statistic will be indicated by the subscripts 's' for space and 't' for time, respectively. For example, $MEAN_s(E)$, which is identical to ME_s, denotes the spatial mean error, whereas $COR_s(TREND_t)$ denotes the spatial correlation between the cross-validated and observed temporal trends.

3. RESULTS

3.1. Temperature

3.1.1. Cross-validation results and analyses of station data

Fig. 4a shows the spatial distribution of the cross-validated errors obtained for the annual mean $\overline{T}$ ($\overline{T}_{Ann}$), as computed from the monthly values. It can be seen
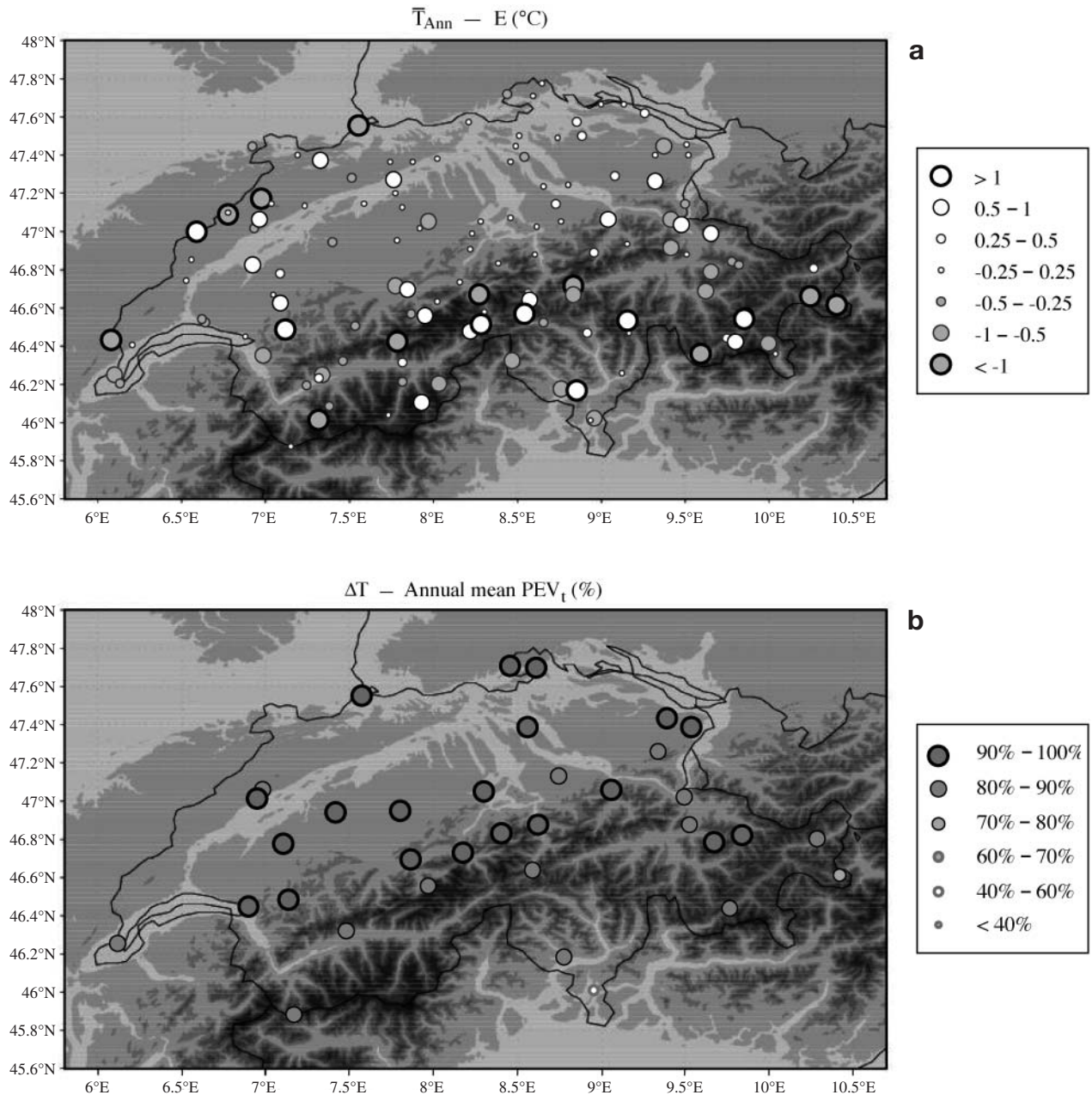
Fig. 4. Cross-validation results for (a) the interpolated long-term mean annual mean temperatures ($\overline{T}_{Ann}$, results refer to 1961–1990) and (b) the monthly mean temperature anomalies (ΔT, results refer to 1951–2000). E: Error; PEV_t: proportion of explained temporal variance
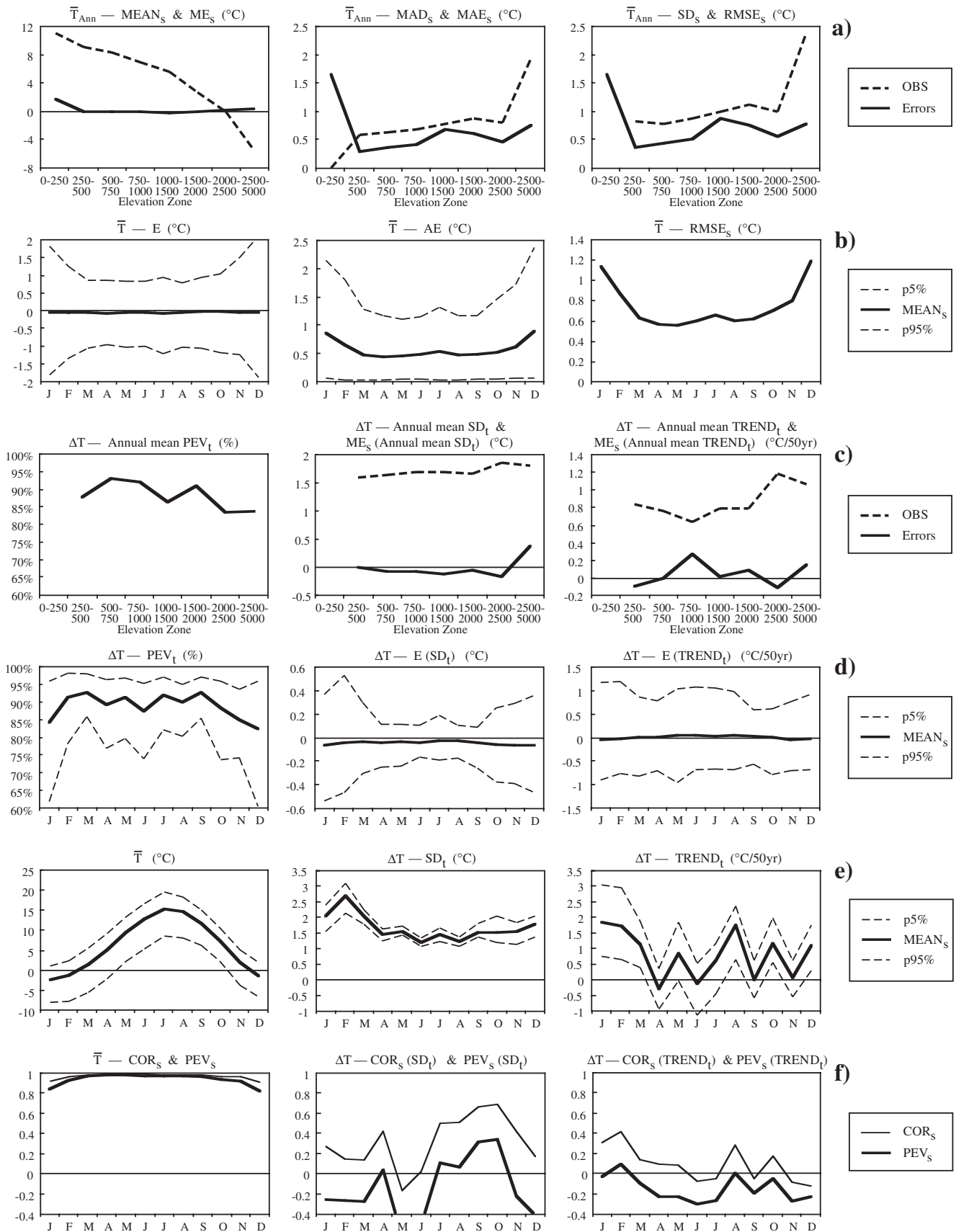
Fig. 5. Cross-validation statistics for the interpolated temperatures and comparison with corresponding statistics derived from the climate station data (OBS). $\overline{T}_{Ann}$: long-term mean annual mean temperature; $\overline{T}$: long-term mean monthly mean temperature (n = 136 climate stations, data refer to 1961–1990); ΔT: monthly temperature anomaly (n = 35 climate stations, data refer to 1951–2000). (a,b) Results for the interpolation of $\overline{T}$ as a function of elevation and month; (c,d) results for the interpolation of ΔT as a function of elevation and month; (e) observed monthly statistics; (f) monthly pattern similarities between the station data and the cross-validation results. For the abbreviations used to denote the various error and data statistics see Table 4; subscripts s and t denote space and time, respectively

◄──

that 90% of all errors were less than 1°C. Fig. 4b shows the spatial distribution of the PEV_t statistic for the cross-validated annually averaged ΔT. Here a north-south gradient can be discerned. The average value from all stations was 89%; the smallest value (41%) was obtained for Lugano in southern Switzerland.

The errors for $\overline{T}_{Ann}$ depended only weakly on elevation (Fig. 5a). ME_s was generally below 0.3°C, except for the lowest and highest elevation zones, where it amounted to +1.66 and +0.44°C, respectively. Note, however, that for these elevation zones only 1 and 3 stations, respectively, were available (Fig. 1). MAE_s and $RMSE_s$ were both generally well below 1°C, and for elevations above 250 masl always smaller than MAD_s and SD_s, respectively, of the measured data.

Fig. 5b shows selected error statistics for $\overline{T}$ as a function of month. ME_s was close to zero for all months. MAE_s and $RMSE_s$ showed a distinct annual cycle, with high values in the winter half-year and lower values in the summer half-year. Mean MAE_s for October to March was 0.67°C, whereas the average value for the remaining months was 0.48°C. Annually averaged $RMSE_s$ for $\overline{T}$ was 0.75°C.

Fig. 5c refers to the interpolation of ΔT. Annually averaged monthly PEV_t showed a slight decrease with elevation. The annual mean SD_t was underestimated for all elevations zones below 2500 masl, by on average –0.1°C or –4%, and it was overestimated at the one available location above 2500 masl (Jungfraujoch, 3580 masl), by 0.37°C or 20%. ME_s for annual mean $TREND_t$ was below 0.3°C per 50 yr for all elevation zones, and generally it was much smaller than the observed average trends.

The monthly cross-validation statistics for ΔT are shown in Fig. 5d. Monthly PEV_t values were mostly above 87%, except for November to January (82 to 85%). For SD_t the annual mean ME_s and MRE_s amounted to –0.05°C and –2%, respectively. The absolute errors (not shown) were generally smaller for the summer half-year compared with the winter half-year: April to September mean MAE_s ($MARE_s$) amounted to 0.09°C (6.3%), whereas for the remaining months it was 0.2°C (10.6%). Annual mean ME_s for $TREND_t$ was 0.1°C. The errors showed the largest spatial variability for January, February and May (90% range: ~2°C). Annual mean MAE_s amounted to 0.43°C.

The $MEAN_s$ and the 5 and 95% percentiles of $\overline{T}$ from 136 climate stations are shown in Fig. 5e. The long-term mean temperatures varied between 2.3°C (January) and 15.2°C (July). Annual mean SD_s of $\overline{T}$ was 3.4°C. Areal mean SD_t and its spatial variability also showed a clear seasonal signal: both were smallest during spring and summer. Quite differently, the 50 yr areal mean trends showed a very jagged annual cycle. The largest trends were on the order of the mean SD_t. They occurred for January (+1.84°C per 50 yr), followed by August (+1.76°C per 50 yr) and February (+1.71°C per 50 yr). Negative mean trends were obtained for April (–0.29°C per 50 yr) and June (–0.13°C per 50 yr).

Fig. 5f shows how the spatial variability of the measured statistics relates to the amplitudes of the cross-validated errors. With regard to $\overline{T}$, large positive values were obtained for both measures of spatial coherence used, COR_s and PEV_s. The $\overline{T}$ pattern was better reproduced from March to September (PEV_s = 0.81 to 0.86) than from the remaining months (PEV_s = 0.58 to 0.75). The PEV_s statistics for monthly SD_t and $TREND_t$ were generally below zero. However, COR_s was positive in several cases, thus indicating some similarity in the spatial pattern of the observed and cross-validated data.

3.1.2. Comparison of interpolation methods

The use of a simple linear regression to predict $\overline{T}$ from elevation yielded practically the same results (Fig. 5a,b,f) as the newly proposed method (comparison not shown).

The cross-validation results of the newly proposed method and of the IDW method are compared in Fig. 6. The results shown for IDW are only for the case $\alpha = 2.0$, which gave the best average performance for all months.

It can be seen that the local temporal variability of ΔT was reproduced roughly equally well by both procedures, except for October to December, for which time the new procedure yielded somewhat better results (Fig. 6a). The spatial variability of the ΔT anomaly fields was better reproduced by the new procedure for September to February, but IDW proved to be superior from April to June (Fig. 6b).
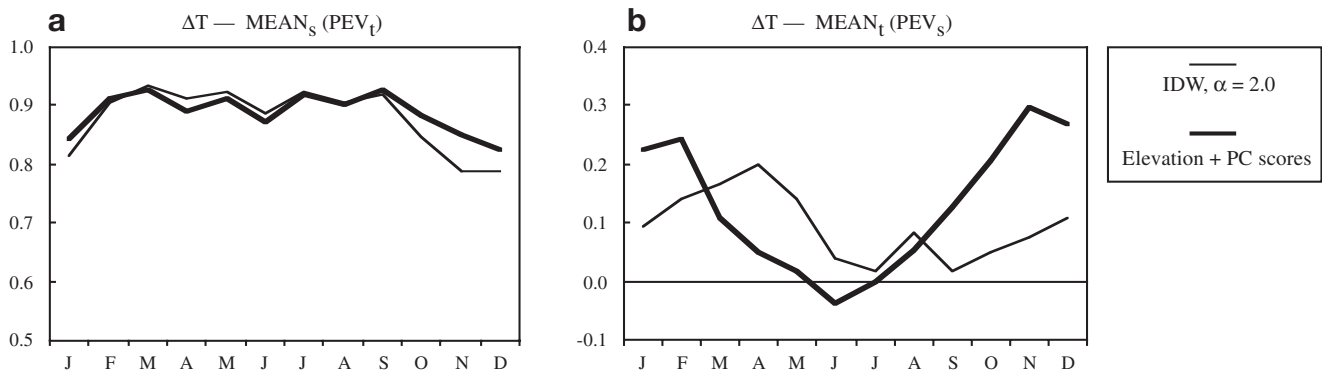
Fig. 6. Comparison of cross-validation results for the inverse distance weighting (IDW) and the orographically based (elevation + PC scores) interpolation procedures. ΔT: monthly temperature anomalies (results refer to 1951–2000); (a) $MEAN_s$: spatial mean; PEV_t: proportion of explained temporal variance; (b) $MEAN_t$: temporal mean; PEV_s: proportion of explained spatial variance

3.1.3. Interpolation results

Fig. 7 shows the results obtained from the newly proposed interpolation procedure for seasonal mean $\overline{T}$ (Fig. 7, left-hand panels) and the seasonal mean SD_t (Fig. 7, right-hand panels), which was computed from the monthly ΔT fields. As could be expected (Fig. 5e) both parameters showed a distinct annual cycle, and the mean temperatures showed a strong influence of the relief (cf. Fig. 2).

Fig. 8 compares the measured seasonal mean temperature trends for 1951–2000 with the trends that were derived from the monthly interpolated ΔT fields.

The station data (Fig. 8, left-hand panels) generally showed positive trends, which were largest for winter and summer (cf. Fig. 5e). However, no clear spatial pattern can be discerned, except perhaps for a tendency towards stronger warming in the eastern part of Switzerland in winter. Negative seasonal mean trends were found at a few isolated locations for spring, summer and autumn. For all seasons there were cases where the trends between neighboring sites just a few tens of km apart differed by more than 1 to 2°C per 50 yr (cf. the wide 90% range shown in Fig. 5e).

The interpolated trend maps (Fig. 8, right-hand panels) reflected the general characteristics of the station data. However, the interpolated fields showed smoother horizontal gradients compared with the measurements, and they displayed a clearer orographic signal. For example, for all seasons the interpolated maps depicted relatively large trends over the Jura Moun-

tains in west-northwest Switzerland. Substantial differences were found between the observed and interpolated trends at individual locations; several negative station trends cannot be discerned in the interpolated fields (cf. relatively large variance of errors in Fig. 5d).

3.2. Precipitation

3.2.1. Cross-validation results and analyses of station data

The spatial distribution of RE for the long-term mean annual total precipitation ($\overline{P}_{Ann}$), as computed from the monthly cross-validated values, is shown in Fig. 9a. The MRE_s for the 511 stations considered was 1.2%. Large errors were obtained at higher elevations and towards the margins of the study area. The 2 largest errors occurred at the sites Campocologno (535 masl, marked with an '$\mathbf{x}$' in Fig. 9a; RE = –100%) and Corvatsch (3315 masl, located NW of Campocologno; RE = +85%). For 90% of all other locations the RE for $\overline{P}_{Ann}$ was below 20%.

Fig. 9b shows the distribution of the annually averaged PEV_t for ΔP. The mean PEV_t from the 143 stations considered amounted to 74%. Again, errors tended to increase with elevation, and particularly large errors were obtained at 3 isolated sites, which are marked with an '$\mathbf{x}$'. They were (from west to east in Fig. 9b): Zermatt (1638 masl, –321%), Scuol (1295 masl, –243%) and Santa Maria (1390 masl,

Fig. 7. Seasonal mean temperature (left-hand panels) and seasonal mean standard deviations of monthly mean temperature (right-hand panels) as computed from the interpolated fields. $\overline{T}$: long-term mean monthly mean temperature (data refer to 1961–1990); ΔT: monthly mean temperature anomaly (data refer to 1951–2000); DJF: December–February; MAM: March–May; JJA: June–August; SON: September–November. Circles denote the locations of the stations used for interpolation

$\overline{T}$ – DJF mean

ΔT – DJF mean SD_t

$\overline{T}$ – MAM mean

ΔT – MAM mean SD_t

$\overline{T}$ – JJA mean

ΔT – JJA mean SD_t

$\overline{T}$ – SON mean

ΔT – SON mean SD_t

−10 −8 −6 −4 −2 0 2 4 6 8 10 12 14 16 18 20
(°C)

1 1.125 1.25 1.375 1.625 1.75 1.875 2 2.125 2.25 2.375 2.5 2.75 2.875 3
(°C)

ΔT – DJF mean TREND_t

ΔT – MAM mean TREND_t

ΔT – JJA mean TREND_t

ΔT – SON mean TREND_t
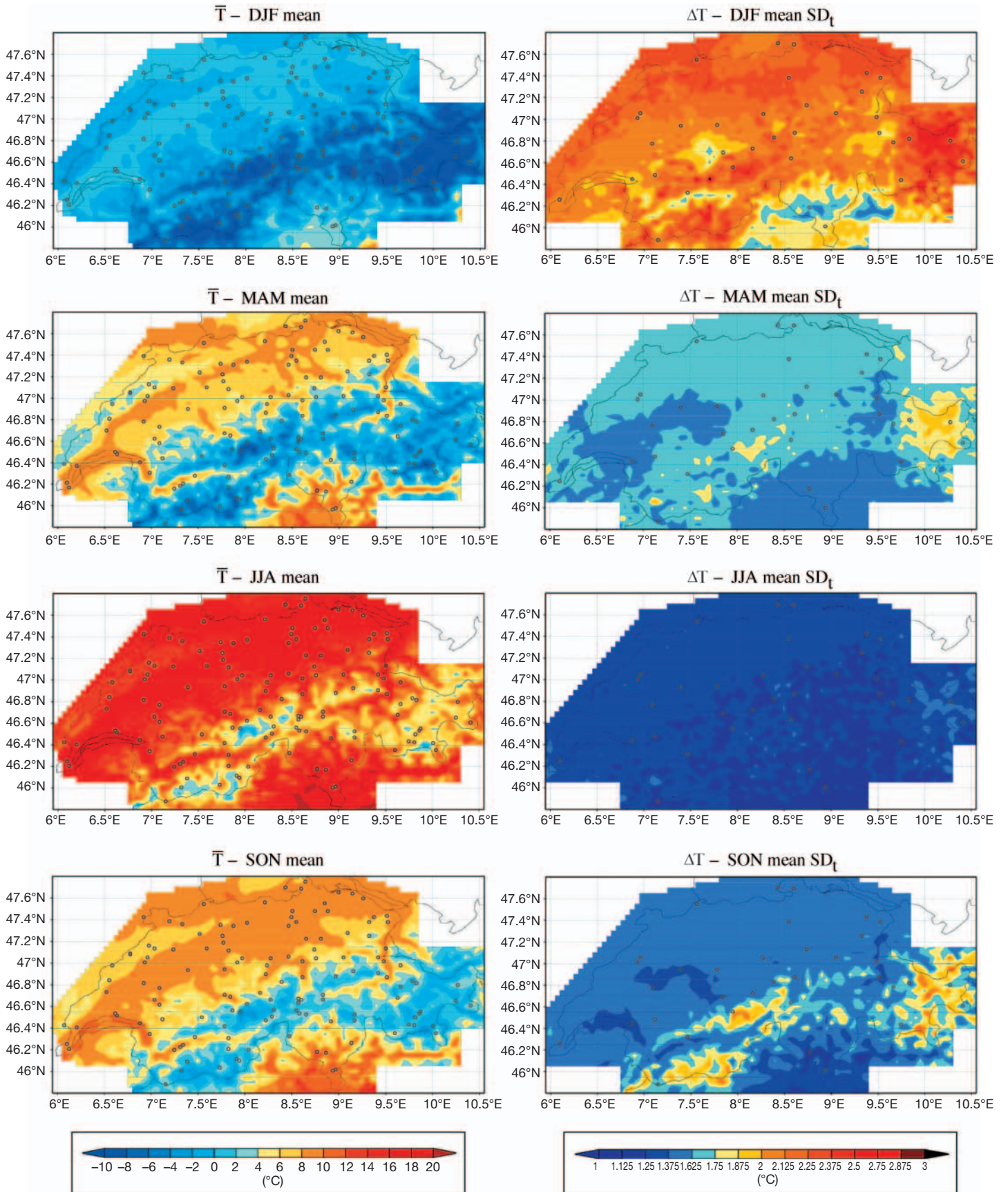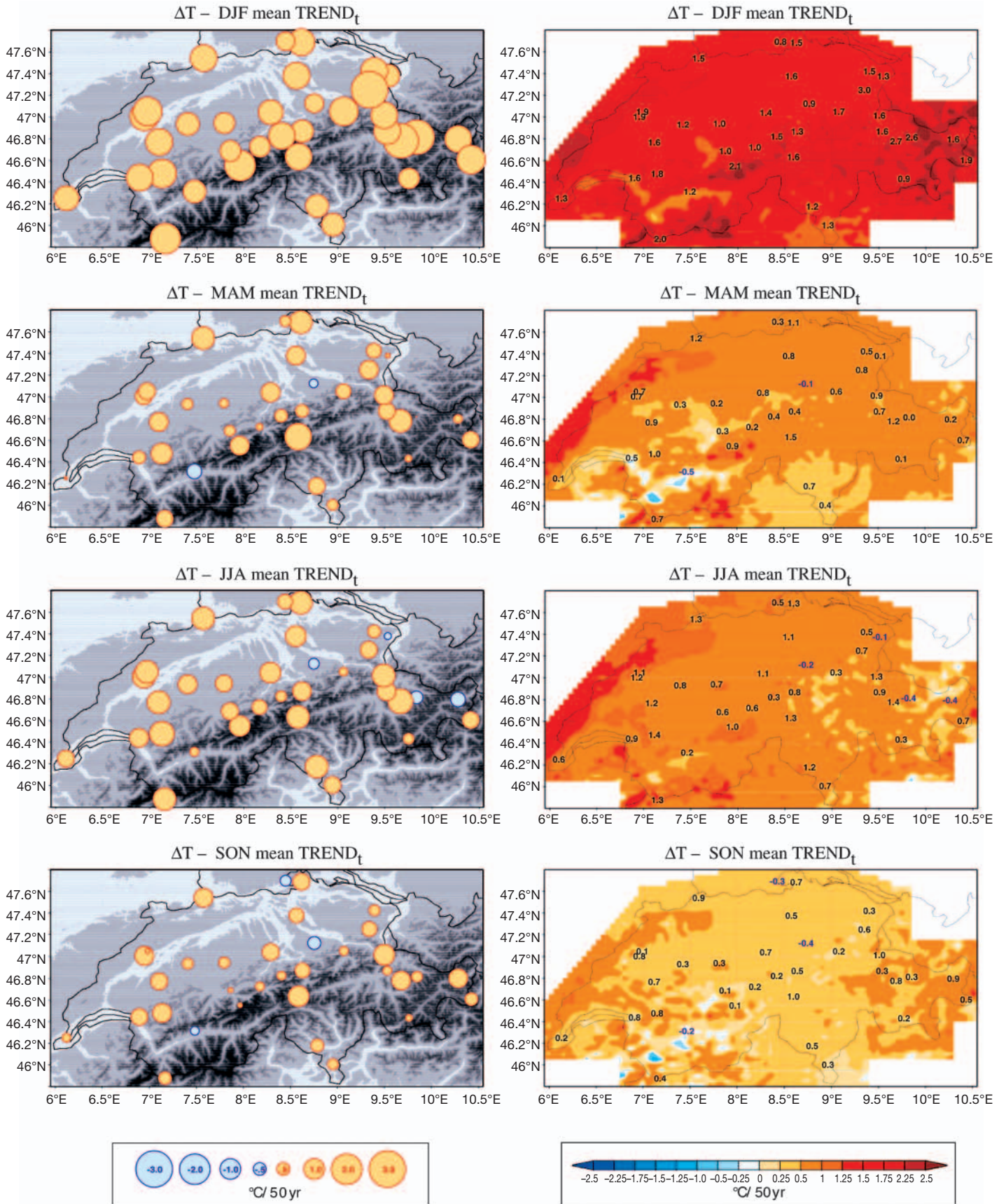
Fig. 8. Comparison between measured seasonal mean trends of monthly mean temperatures (left) with trends derived from the interpolated fields (right). ΔT: monthly mean temperature anomaly (data refer to 1951–2000)

◄─────────────────────────────────────

–238 %). These stations were excluded from the calculation of all further cross-validation statistics. The average PEV_t without the 3 outliers was 81 %.

The altitudinal distribution of the errors for $\overline{P}_{Ann}$ is shown in more detail together with some statistics of the observed data in Fig. 10a. ME_s was generally a few mm per year for elevations below 1500 masl. MRE_s was

1 to 2 %. Much larger values were obtained for the elevation zones 2000–2500 masl (7 stations; Fig. 1) and above 2500 masl (2 stations), where MRE_s amounted to –10 and +47 %, respectively. MAE_s and $RMSE_s$ showed a clear increase with elevation. Above 2000 masl the cross-validated errors surpassed the observed variability as measured by MAD_s and SD_s.
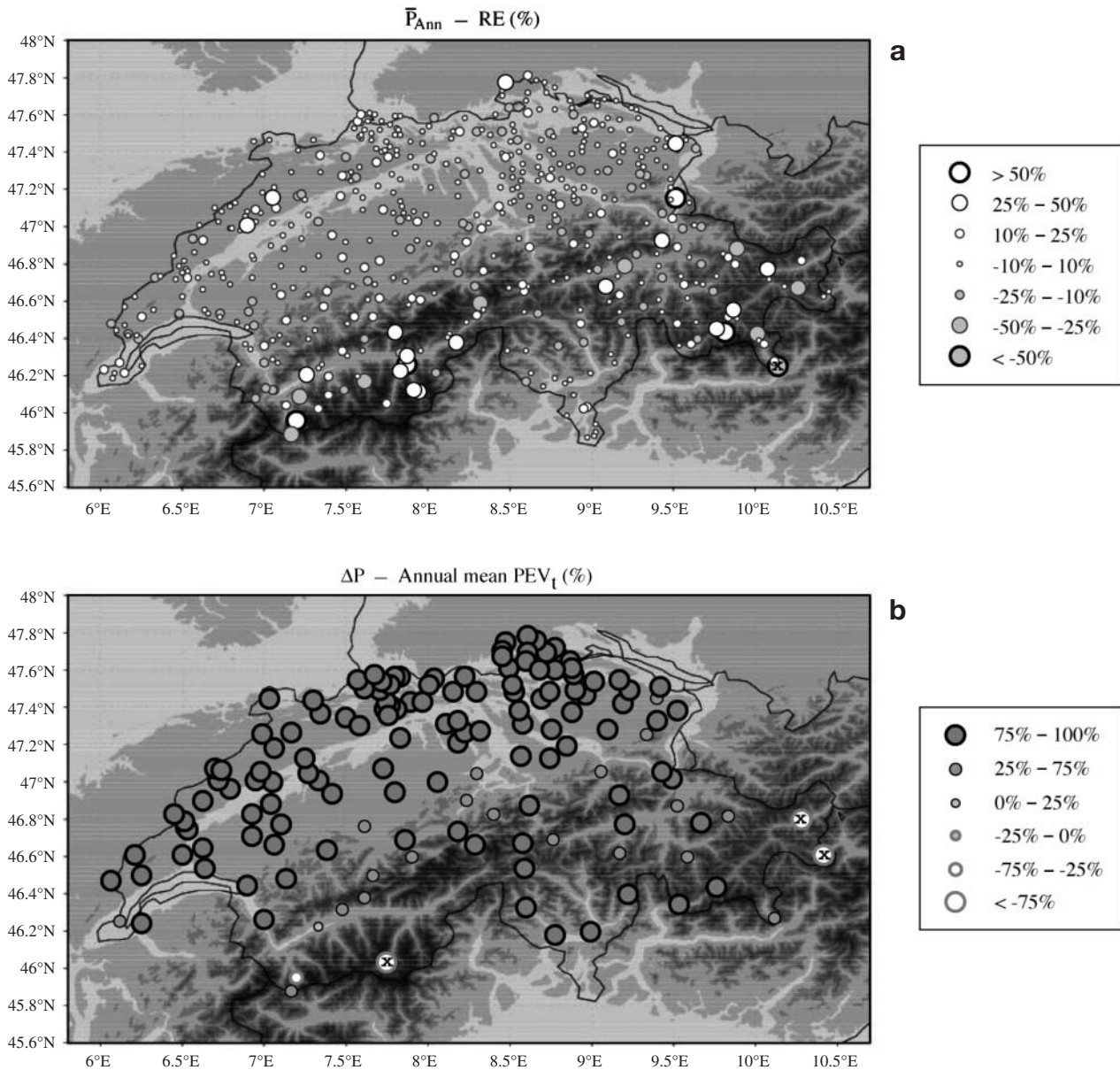
Fig. 9. Cross-validation results for (a) the interpolated long-term mean annual total precipitation ($\overline{P}_{ANN}$, results refer to 1961–1990) and (b) the monthly precipitation anomalies (ΔP, results refer to 1951–2000). RE: relative error; PEV_t: proportion of explained temporal variance. Stations marked with an 'X' showed very large errors and were excluded from all further analyses of cross-validation results (see also text)
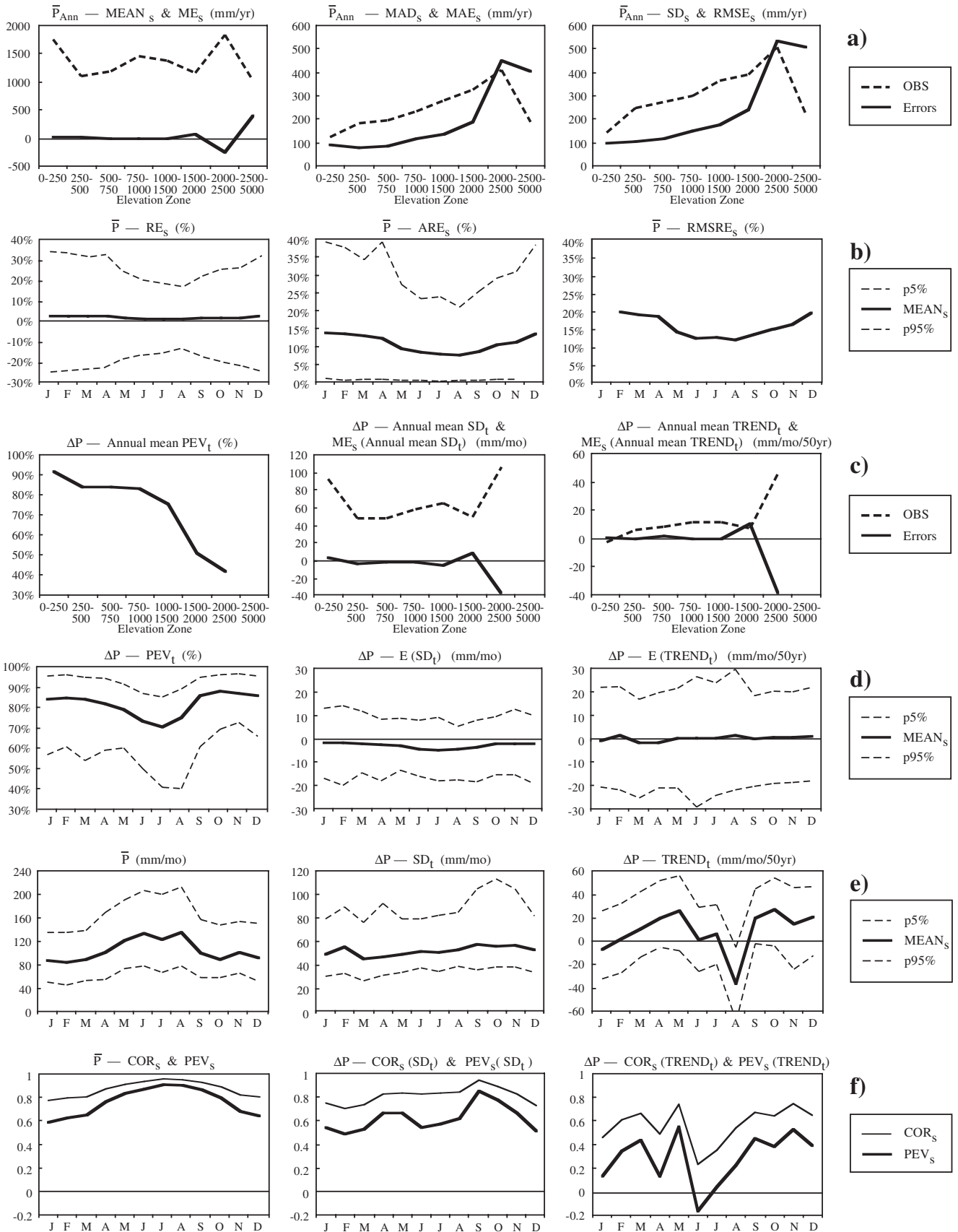
Fig. 10. Cross-validation statistics for the interpolated precipitation totals and comparison with corresponding statistics derived from the climate station data (OBS). $\overline{P}_{Ann}$: long-term mean annual total precipitation; $\overline{P}$: long-term mean monthly total precipitation (n = 511 climate stations, data refer to 1961–1990); ΔP: monthly precipitation anomaly (n = 143 climate stations, data refer to 1951–2000). (a,b) Results for the interpolation of $\overline{P}$ as a function of elevation and month; (c,d) results for the interpolation of ΔP as a function of elevation and month; (e) observed monthly statistics; (f) monthly pattern similarities between the station data and the cross-validation results. For the abbreviations used to denote the various data and error statistics see Table 4; subscripts s and t denote space and time, respectively

The annual cycles for the mean and 5 and 95% percentiles of 3 relative error measures for $\overline{P}$ are shown in Fig. 10b. Averaged over the whole year MRE_s amounted to +2%, $MARE_s$ to 11%, and $RMSRE_s$ to 16%. The annual mean ME_s, MAE_s and $RMSE_s$ amounted to 0.0, 10.5, and 15.3 mm mo^{-1}, respectively. All statistics suggested increased accuracy of the interpolation procedure during the summer compared with the winter.

Fig. 10c summarizes the cross-validation results for ΔP as a function of station elevation. Note that no stations were available above 2500 masl (Fig. 1). Annual mean PEV_t showed a clear decrease with elevation. The average value from the 4 (2) considered stations in the elevation zones 1500–2000 masl (2000–2500 masl) was 50% (42%). These elevation zones also showed the highest ME_s for annual mean SD_t and $TREND_t$.

Fig. 10d shows the monthly PEV_t statistics. It can be seen that from March to August the temporal variability was less well reproduced compared with the other months. SD_t showed a slightly negative ME_s. On average over all months it amounted to –1.9 mm mo^{-1}. The annual mean MRE_s, MAE_s and $MARE_s$ for SD_t were –3%, 7.1 mm mo^{-1} and 13%, respectively (not shown). ME_s for $TREND_t$ was generally small and showed no clear seasonal cycle.

The distribution of the measured $\overline{P}$ data is shown in Fig. 10e. The annual mean from all 511 stations was 105 mm mo^{-1} (or 1260 mm yr^{-1}). The largest areal mean values were found for June and August (135 mm mo^{-1}), and the smallest for February (84 mm mo^{-1}). The inter-station variability (dashed lines in Fig. 10e) followed the mean and was largest for April to August. The annual mean SD_s was 33.3 mm mo^{-1}.

The SD_t statistics for the station data are also shown in Fig. 10e. The average SD_t from all stations showed an annual mean value of 52 mm mo^{-1} and a moderate seasonal cycle. The spatial variability of SD_t varied more strongly and showed maxima in February, April and September to November.

The mean $TREND_t$ from all stations varied strongly with the time of the year. It was positive for all months, except for January (–6.8 mm mo^{-1} per 50 yr) and August (–37 mm mo^{-1} per 50 yr). The variability between stations (dashed lines in Fig. 10e) was considerable, except for August to October, for which time trends of common sign were found at most stations.

The interpolation method's ability to reproduce the spatial distribution of selected precipitation parameters is assessed in Fig. 10f. For $\overline{P}$ the pattern similarity between the cross-validated and measured data was generally high and showed a clear annual cycle with maximum values in the summer half-year. The spatial variability of SD_t and $TREND_t$ was less well reproduced. However, the error statistics suggested reasonable skill for all months, except perhaps for $TREND_t$ in June and July.

3.2.2. Comparison of interpolation methods

Fig. 11a,b compares the performance of the REP, the PRISM and the newly proposed method for the interpolation of $\overline{P}$. REP gave generally large ME_s and MAE_s values for all elevation zones compared to the other 2 methods. PRISM and the newly proposed method performed equally well for elevations ≤2000 masl, but for the elevation zone 2000–2500 masl PRISM clearly gave the best results.

The cross-validation results of the newly proposed method and the IDW method with regard to ΔP are compared in Fig. 11c,d. Again, IDW clearly performed best for $\alpha = 2.0$, such that only this case is reported here.

It can be seen that generally both the temporal (Fig. 11c) as well as the spatial (Fig. 11d) variability of the anomaly fields was better reproduced by the IDW interpolation. The differences between the 2 methods were largest for March to September.

3.2.3. Interpolation results

Seasonal averages of the interpolated monthly $\overline{P}$ fields are shown in Fig. 12, left-hand panels. It can be seen that summer is the wettest season over most of the area. In the Ticino region, southern Switzerland (subsectors 4.5 and 5.5; Fig. 2), large average precipitation amounts can also be observed in the transition seasons. Maxima were obtained for all seasons over the Jura Mountains (subsectors 3.1, 2.2 and 2.3), and along the main Alpine ridge. The minima were found in the interior of the mountain range, in Valais (subsectors 4.3 and 4.4) and southeastern Switzerland (subsector 5.3).
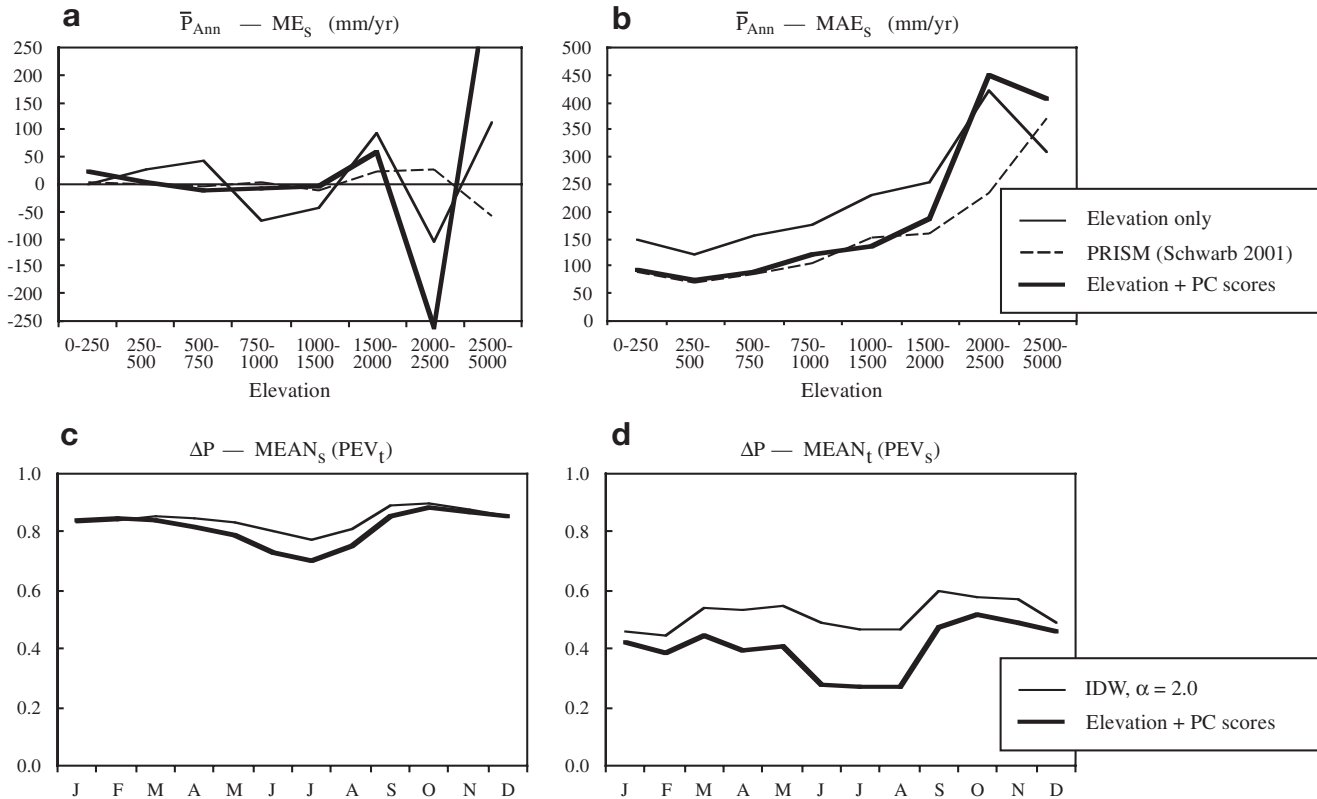
Fig. 11. Comparison of cross-validation results obtained from different interpolation procedures. (a) $\overline{P}_{Ann}$: long-term mean annual total precipitation (results refer to 1971–1990 for PRISM and to 1961–1990 for the other procedures); ΔP: monthly precipitation anomalies (all results refer to 1951–2000); ME_s: spatial mean error; (b) MAE_s: spatial mean absolute error; (c) $MEAN_s$: spatial mean; PEV_t: proportion of explained temporal variance; (d) $MEAN_t$: temporal mean; PEV_s: proportion of explained spatial variance

Fig. 12, right-hand panels shows the 50 yr, seasonally averaged interannual standard deviations of ΔP, as computed from the interpolated monthly anomaly fields. The largest SD_t values were generally obtained in the southern part of the study region. Large interannual variability was also found for the main Alpine ridge and the Jura Mountains during winter and autumn.

The seasonally averaged, measured and interpolated ΔP trends are juxtaposed in Fig. 13. The measurements (Fig. 13, left-hand panels) showed for the transition seasons positive, for summer negative, trends at most locations. For winter a more complex pattern was found, with positive trends in the northwest and southwest, negative trends in the south-southeast of the study domain, and trends of oscillating sign along the main Alpine ridge and its northern rim.

The trend maps (Fig. 13, right-hand panels) picked up the main features of the observations for all seasons. However, as this was the case for temperature, major deviations from the measurements occurred at the locations of individual climate stations. An example are the summer trends for subsector 3.5 (Fig. 2), where most stations showed decreasing trends, whereas the interpolated map suggested a slight increase in seasonal mean precipitation.

4. DISCUSSION

Several climatological data sets similar to the one derived here have already been produced for the Alpine and Swiss regions (Table 1). However, to my knowledge, this is the first study to provide a multi-

Fig. 12. Seasonal mean precipitation totals (left-hand panels) and seasonal mean standard deviations of monthly precipitation totals (right-hand panels) as computed from the interpolated fields. $\overline{P}$: long-term mean monthly total precipitation (data refer to 1961–1990); ΔP: monthly precipitation anomaly (data refer to 1951–2000). Circles denote the locations of the stations used for interpolation

$\overline{P}$ – DJF mean
ΔP – DJF mean SD$_t$
$\overline{P}$ – MAM mean
ΔP – MAM mean SD$_t$
$\overline{P}$ – JJA mean
ΔP – JJA mean SD$_t$
$\overline{P}$ – SON mean
ΔP – SON mean SD$_t$

20 40 60 80 100 120 140 160 180 200
mm mo^{-1}

20 40 60 80 100 120 140 160 180 200
mm mo^{-1}
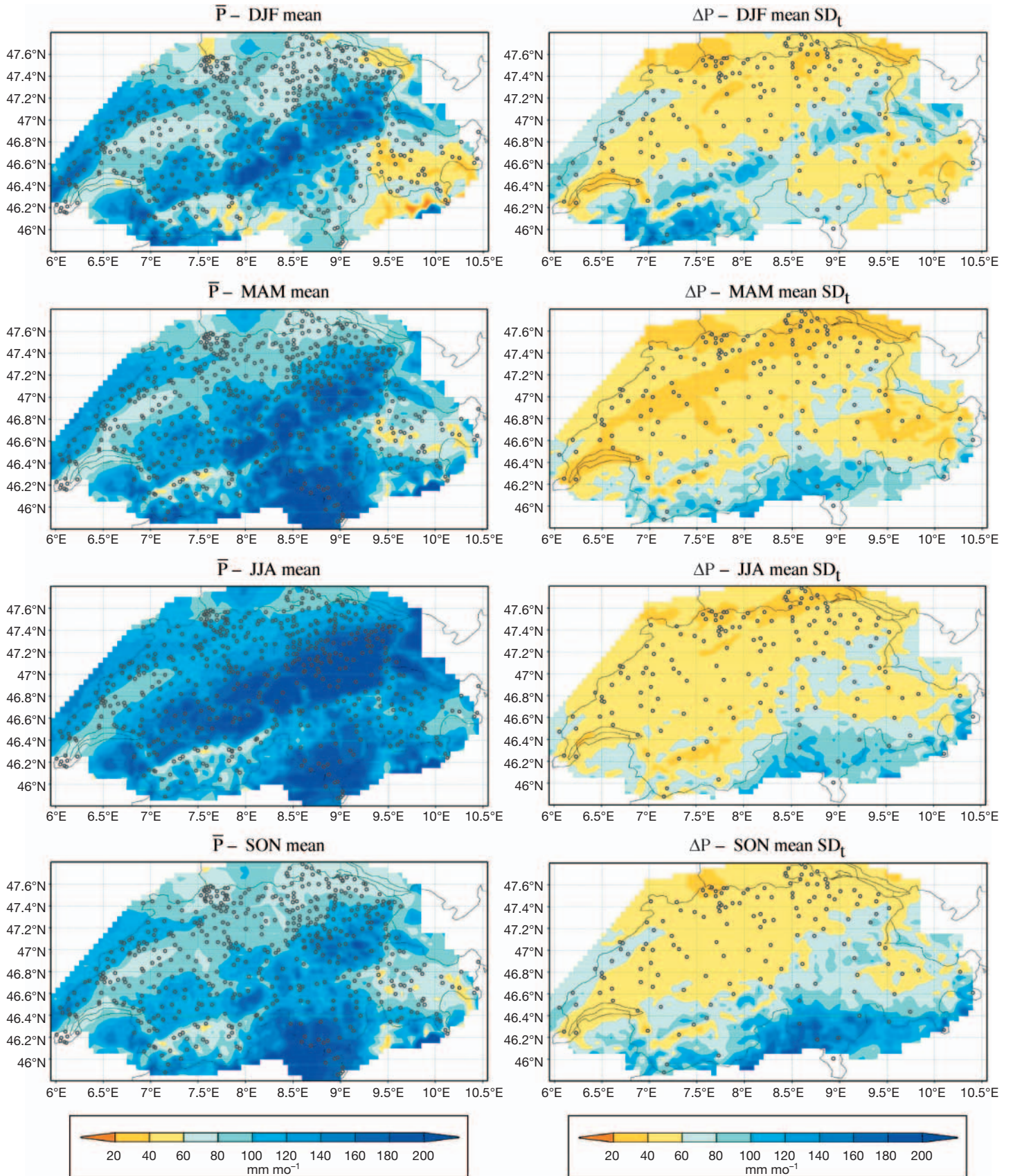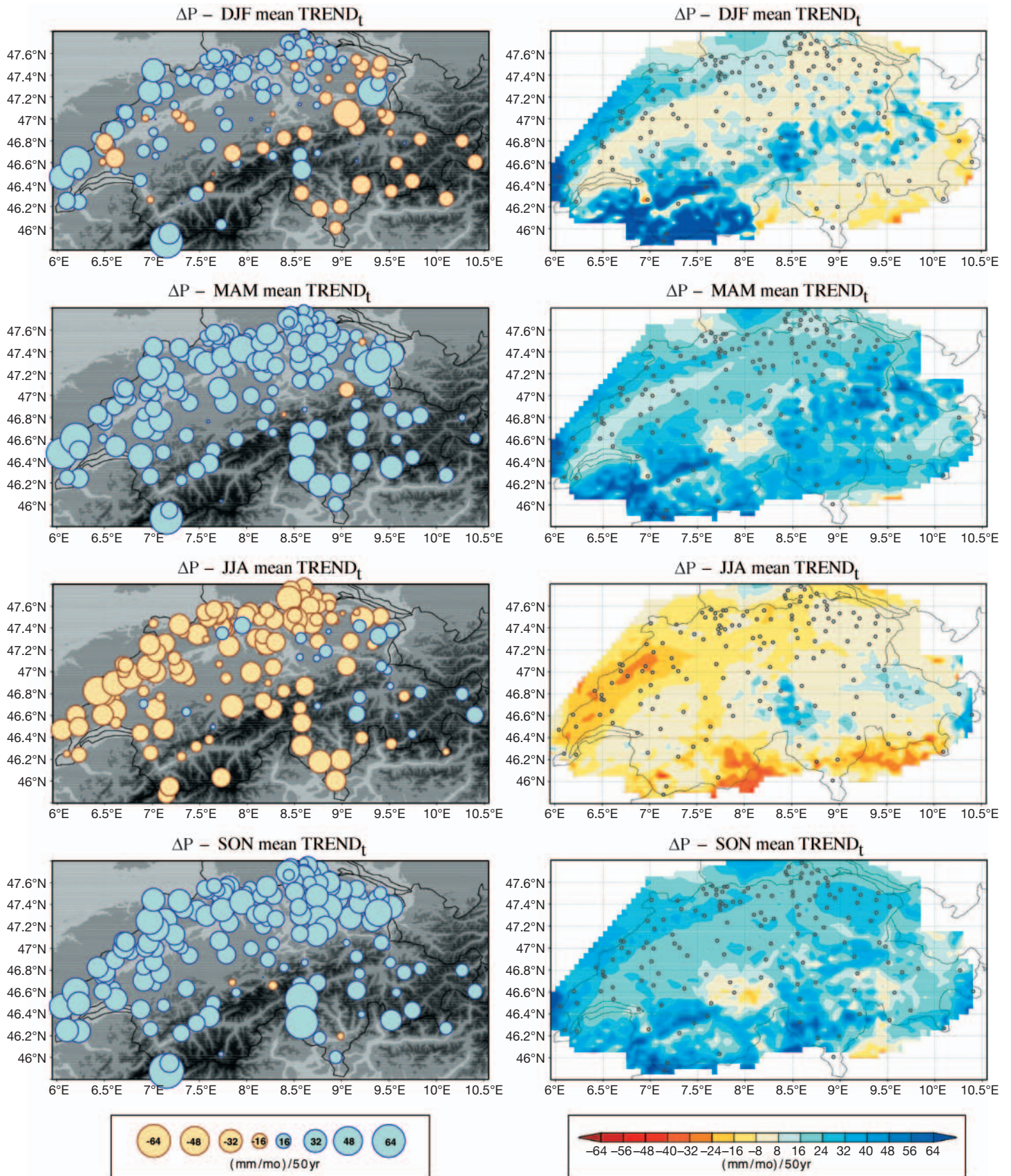
Fig. 13. Comparison between measured trends for seasonal precipitation totals (left-hand panels) with trends derived from the interpolated fields (right-hand panels). ΔP: monthly precipitation anomaly (data refer to 1951–2000)

variable, multi-decadal, consistent data set at a 5 km resolution.

The main purpose of this work was to derive a relatively comprehensive description of the Swiss climate and the associated error bars, rather than to optimize every single aspect of the interpolated data set. Many improvements are certainly possible, and the following subsections will discuss in turn issues related to the data set's resolution, to the data and method employed, and to the accuracy and utility of the results.

4.1. Resolution issues

Unlike many earlier studies (e.g. Nos. 2, 4, 5, 8, 10, 13 and 14 in Table 1) the present work did not consider grids of areal mean values, but rather it aimed at estimating the amplitude of various scalar fields F at unsampled locations (Eq. 2).

Whereas the accuracy of interpolated areal mean data is typically limited by the number and representivity of the climate stations available in the vicinity of each gridbox, the problem encountered here was that a station network with average distance $\overline{D}_s$ between neighboring stations can only resolve spatial variations in F of scale $\geq 2\overline{D}_s$. In this study $\overline{D}_s$ was between 5.1 (for $\overline{P}$) and 24 km (for ΔT), so one might ask whether there were enough data to support a 5 km resolution.

At least 2 answers can be given to this question. Firstly, from a pragmatic point of view, one may argue that it is always better to have some objectively derived estimate of F at unsampled locations rather than none at all, provided that the associated error bars (Figs. 5 & 10) are kept in mind by the users of the data set. Secondly, and more importantly, the present work aimed precisely at exploiting the additional information provided by appropriate covariates (Fig. 3c,d; top 2 rows in Table 3) in order to enhance the limited resolution of the station data.

Having a gridpoint distance $\overline{D}$ of 5 km, the derived data set in principle resolves variations in F of scale $\geq 2\overline{D} = 10$ km. Of course, the true behavior of F is masked by interpolation errors, and users of the data set are advised to trust only differences between locations that are well above the typical MAE or RMSE values that are reported in Figs. 5 & 10. Nevertheless, note that the mean cross-validated errors were typically close to zero (Figs. 5a,b,d & 10a,b,d), such that on average the interpolated surfaces can be expected to correctly reproduce the true F. An exception applies to $\overline{P}$, and perhaps also to ΔP, for elevations above 2000 masl, where larger systematic errors were found.

Several applications require site-specific data at a much higher resolution than 5 km. The gridpoint distance of the present data set could easily be enhanced to 1 km, since all needed covariates were available at this resolution (Fig. 3). The present work employed a 5 km grid only for purely technical reasons, in order to save computing time and reduce storage requirements. The production of grids with $\overline{D}_{GP} < 1$ km is, however, presently not possible with the proposed method, due to the lack of appropriate DEM data outside of Switzerland.

Some applications, such as the validation of climate models, require grids of areal mean values with a resolution of 25 to 50 km. Such grids can be easily produced from the present data set by averaging all gridpoints found in a target gridbox. Note that this is likely to improve the accuracy of the data set, because the interpolation error at each gridpoint can be viewed as a random variable with a zero mean (in most cases, see above) and a standard deviation $s \approx$ RMSE (as defined in Table 4); and according to standard statistical theory, the mean of n identically distributed, independent random variables has a standard deviation of $s/\sqrt{n}$. Hence, the transition to a 25 km (or 50 km) grid implies an error standard deviation for the gridbox mean of $s/5$ (or $s/10$). Somewhat larger values must be expected if the errors at neighboring gridpoints are correlated.

Schmidli et al. (2001) give an example of this effect. They reported a strong improvement in the representation of temporal variability when they considered regional means from several gridpoints of their 25 km Alpine-wide precipitation data set.

This reduction of the interpolation error variance should, however, not divert attention from a possible sampling problem associated with the 5 km (or any other) grid: given the complexity of the Swiss terrain, it is not clear how many point estimates are actually required per 25 km or 50 km gridbox to correctly capture the areal mean signal. This issue and the spatial covariance structure of the errors remain to be examined in future work.

4.2. Data problems

Data problems related to both the climate station data and the DEM input data might have affected the quality of the interpolations.

Interpolation errors tended to increase towards the south-southeast borders of Switzerland (Figs. 4 & 9) and with elevation (Figs. 5a,c & 10a,c). This was probably due to the low station densities in the respective

regions and elevation zones (see also Fig. 1). The efforts needed to obtain additional data, in particular for Italian stations to the south of Switzerland and for the entire 1951–2000 (or even only the 1961–1990) period, were, however, far beyond the scope of the present study. With regard to precipitation, the data coverage could improve, thanks to possible future updates of the database by Frei & Schär (1998)—the database presently covers only 1971–1990; with regard to temperature, however, no corresponding data-gathering effort seems to be currently on the way.

The interpolation of the anomaly fields was based on a relatively small number of stations that had continuous data for 1951–2000. Data from many other shorter-term Swiss stations are actually available and could have been used to improve the interpolation results for individual months or years. These data were, however, not included because priority was given to producing a temporally homogeneous data set. Moreover, the use of a temporally varying database would have complicated the description and analysis of the interpolation errors, which already show a very complex pattern (Figs. 4, 5, 9 & 10). An alternative to using a time-varying station network, which was not pursued here, would have been to employ record extension techniques (e.g. Hirsch 1982) in order to produce a denser station network for 1951–2000.

A further problem relates to possible inhomogeneities of the station data. Schmutz (2001) analyzed 114 long-term Swiss precipitation stations and concluded that only 39 should be used for long-term trend analyses. He considered 1901–1995, but, unfortunately, he did not report on the time points at which the inhomogeneities were detected. One might speculate that the post-WWII data used in the present study should be more reliable than those considered in his analysis. With regard to temperature, no study similar to Schmutz's seems to have been carried out until now.

The strategy pursued to quantify the effects of possible inhomogeneities by means of cross-validation had the disadvantage that it does not allow separation of poor performance due to data problems from other factors that influence the quality of the interpolations. Also, this strategy might fail to give large cross-validation errors if a large number of neighboring stations show the same kind of inhomogeneity. However, such a configuration would probably also go undetected through a homogeneity test.

The cross-validation procedure might also fail to account for any systematic measurement errors if they occur at a larger number of stations. For precipitation rain gauges, undercatch can lead to errors on the order of several 10% (Sevruk 1985), in particular, at high elevations. The present data set does not consider any corrections for such errors.

A too-coarse or erroneous representation of the relief presents a further source of error, in particular for grid-points that are found in the vicinity of narrow valleys or of mountain ridges. It can be expected that the use of a DEM with a gridpoint distance <1 km would give a particularly strong improvement for temperature. This is because in the present study all orographic regressions were determined using local station elevations, whereas for application of the regressions, the point elevations had to be estimated by interpolation from the DEM.

4.3. Methodical considerations

The selection and evaluation of the orographic predictors is not a straightforward task. This work identified fixed sets of predictors related to elevation and the relief (first 2 rows in Table 3), which were then used to fit spatially varying multiple linear regression models. Possible alternative approaches that remain to be explored might consider the stepwise selection of predictors, the inclusion of non-linear terms or transformed predictor variables (Prudhomme & Reed 1999), or the use of the predictors as covariates for kriging (e.g. Phillips et al. 1992), or for kriging with an external drift (e.g. Pardo-Iguzquiza 1998).

The predictors considered in this work accounted for variations in slope and aspect (Fig. 3a), and for the occurrence of troughs and ridges (Fig. 3b) at different spatial scales. Their possible added value is discussed below mainly based on the comparison with the simpler interpolation procedures. A more detailed analysis of the statistical linkages between the PC scores and the various climate parameters could have provided additional insight, but such work was beyond the scope of the present study.

The use of the PC scores in addition to elevation strongly improved the interpolation of $\overline{P}$ (Fig. 11a,b). An exception applies perhaps for elevations above 2000 masl, but here the comparison of the methods is probably not representative due to the very small number of stations available (Fig. 1). The improvement obtained demonstrates once more that precipitation in the Alps depends on slope and shielding effects and shows no simple relationship with elevation (Schüepp et al. 1978, Frei & Schär 1998).

The comparison with the results of Schwarb (2001) (Fig. 11a,b) suggests that with regard to $\overline{P}$ and up to an elevation of 2000 masl the method used here is as good as PRISM (Daly et al. 1994). The better performance of PRISM reported by Schwarb (2001) for the high-altitude zones is probably because he used a much denser station network. Part of the difference may also be because he tested his method for a dif-

ferent period (1971–1990) and for a different sector, which extended beyond the boundaries of Switzerland.

The new method also gave some improvement compared to IDW interpolation for autumn and winter ΔT (Fig. 6). During these seasons, large-scale inversions and cold-air ponds often dominate the Swiss temperature field. Apparently, the orographically based procedure accounts better for such phenomena than the IDW procedure, which depends entirely on exploiting the spatial correlation in the measured data field.

Interestingly, the PC predictors did not bring any improvement with regard to $\overline{T}$. It is not clear whether this was due to the absence of any significant slope/ aspect, etc., effects at the scales investigated (>11 km; Fig. 3) or whether the station network used or the interpolation procedure used simply failed to capture any corresponding signals.

The orographically based interpolation performed clearly less well than the IDW method for spring ΔT (Fig. 6) and for spring to autumn ΔP (Fig. 11c,d). The fact that the IDW interpolation with $\alpha = 2.0$ gave the best results suggests a relatively rapid decline of useful information with distance. Since the orographically based procedure did not account for this effect, and since the better performance of IDW does not necessarily imply the absence of an orographic signal, it is possible that a combination of both approaches would give the best results. This could be accomplished by distance-weighting the climate station data prior to fitting the regressions (Brunsdon et al. 2001), or by interpolating the residuals from the regressions using an IDW or kriging procedure (e.g. Agnew & Palutikof 2000).

A peculiarity of the method used was that every anomaly field was interpolated individually as a function of the relief. Two alternatives would have been (1) to fit 1 orographic regression model per calendar month and then apply it to all anomaly fields of that particular month; or (2) to first interpolate daily fields (e.g. Frei & Schär 1998), and then use them to compute the monthly climate anomalies. Alternative (1) would have required the estimation of a much smaller number of regression parameters than was the case in the present study. This would probably have given more robust regression equations, however, at the expense of assuming a time-invariant relief-predictand relationship for every calendar month. Alternative (2) could possibly have increased the precision of the results, but it would have been computationally much more demanding. Moreover, it would have had to account for the strongly skewed distributions of daily variables. The present study adopted an intermediate solution, but it is not clear whether this was the optimal choice.

The proposed interpolation method could possibly also be improved by tuning the values of all involved parameters (Tables 2 & 3), for instance, based on the minimization of the cross-validation errors; by experimenting with additional predictors, in particular with variables that account for other physiographic factors than the relief, e.g. vegetation type (Zheng & Basher 1996) or lakes (Z'graggen 2001); and finally by including auxiliary meteorological information, for instance that related to weather types (Courault & Monestiez 1999) or to local insolation and cloudiness (Ninyerola et al. 2000).

4.4. Accuracy of results

The accuracy of the interpolations was estimated by means of leave-one-out cross-validation. This approach provided only information for the sites sampled by the station network, such that the various mean error estimates (ME, MAE, etc.) were biased towards the regions of high data density and the lower elevation zones.

Note also that the cross-validation errors reported for individual locations (e.g. Figs. 4 & 9) probably give a too-pessimistic estimate of the true errors in the vicinity of these locations. This is because the inclusion of all stations for the production of the final grids is likely to improve the accuracy of the interpolations around all available data points.

The accuracy of the present data set could have been assessed further based on a comparison with similar products. However, such work is complicated by problems of data accessibility, as well as the use of different databases, study regions, time periods, resolutions and target variables (point vs areal mean estimates) in the various studies (Table 1). Therefore any comparisons had to be limited to the few studies that have reported similar error measures as the ones considered here.

4.4.1. Temperature

The errors obtained for $\overline{T}$ were generally small when compared to the measured spatial variability (Fig. 5a,f). The smallest error amplitudes were obtained for the summer half-year (Fig. 5b), but in relative terms (i.e. compared with the spatial variability of the temperature field) the spatial distribution of $\overline{T}$ was more accurately reproduced from March to September (Fig. 5f).

This seasonal variation of the errors for $\overline{T}$ probably reflects the effect of more frequent temperature inversions during the autumn and early winter months. Inversions are likely to create abrupt horizontal transi-

tions in the temperature field at a 5 km resolution, and they were probably not captured so well by the interpolation procedure.

The temporal variability of ΔT was generally very well reproduced and showed a distinct annual cycle, with the largest error variances occurring from October to January (Figs. 5d & 6). This decrease in performance was probably again related to the reduced vertical mixing of the atmosphere (and hence a decoupling of low- and high elevation sites) during this time of the year.

The spatial variability of the monthly ΔT fields was generally less well reproduced than their temporal variability (Fig. 6a vs b). Note, however, that PEV_t and PEV_s are both relative error measures and that the interpolation procedure had to capture a very small spatial signal compared with a much larger temporal signal: the average temporal standard deviation of ΔT was between 1.2 and 2.6°C (Fig. 5e), whereas the average spatial standard deviation of the individual monthly ΔT fields was between 0.8°C for winter and as small as 0.4°C in summer (analyses not shown).

The fact that both the IDW procedure and the orographically based procedure yielded relatively low PEV_s values points towards the existence of strongly local controls for ΔT that are quite independent of the relief. These might relate to perturbations of the local radiation balance, e.g. due to site-specific cloudiness or boundary-layer effects.

4.4.2. Precipitation

The interpolation errors for $\overline{P}$ were smaller than the measured spatial variability only for elevations below 2000 masl (Fig. 10a). Schwarb (2001) experimented with different interpolation methods and station networks and found that the availability of accurate station data is probably the major factor that controls the quality of statistical interpolations of $\overline{P}$ in the Alps. Schwarb (2001) used a better database than the one that was available for the present study, and his data set is certainly more accurate than the one provided here for elevations >2000 masl (Fig. 11a,b).

The spatial pattern of $\overline{P}$ was clearly better reproduced for summer compared with winter (Fig. 10b,f). Neidhöfer (2000) reported a similar result. This suggests that the relief controls the spatial pattern of the long-term mean precipitation more closely in the warm season compared with the cold season. A possible mechanism could be related to the triggering and propagation of convective weather systems in the vicinity of orographic obstacles, such as the Alpine foothills. Such a long-term orographic signal does not depend on the stochastic nature of individual precipitation events.

The temporal variability of ΔP was generally well reproduced (Figs. 10d & 11c, but note also Fig. 9b). Schmidli et al. (2002) reported similar values (PEV_t > 0.9 along the northern Alpine flank and $PEV_t \approx 0.6$ in the southern parts of the Alps), however, for areal mean anomalies and only at a 25 km resolution.

The temporal skill of the interpolations in the present study was better for the winter season compared with the summer months (Fig. 11c). This was probably because the stronger large-scale forcing during winter yields spatially more coherent climate anomalies, which can be better captured by the interpolation procedure.

As was the case for temperature, the spatial variability of the ΔP fields was generally less well reproduced than their temporal variability (Fig. 11c vs d). The average PEV_s value was 0.4 (Fig. 11d). Schmidli et al. (2002) reported PEV_s values between 0.67 (lower quartile of all monthly fields) and 0.8 (upper quartile) for their monthly Alpine-wide ΔP fields. Similar to the present study (Fig. 11d), they found a somewhat smaller spatial skill for summer. This could be due to the predominance of smaller-scale and more erratic weather systems during the warm season.

In summary, the comparison with the results of Schmidli et al. (2002) suggests that with an increase in spatial resolution (i.e. a decrease of the gridpoint distance from 25 to 5 km) the temporal variability of ΔP is still well reproduced, but that the spatial accuracy of the grids deteriorates.

4.4.3. Standard deviation and trend fields

The relatively poor representation of the spatial variability of the ΔT and ΔP fields affected the accuracy of the derived standard deviation and trend fields, which were also not so well reproduced (Figs. 5f & 10f). The mean errors for the derived fields were, however, in most cases close to zero (Figs. 5c,d & 10c,d). This suggests that the relatively large error variances were not caused by a systematic deviation at all stations, but rather by locally varying errors of opposite sign (see also Figs. 8 & 13).

One reason why the small-scale variability of the station statistics was not so well reproduced was that the orographic regression equations were determined using data from a relatively large number of stations (Table 3). Consequently, the small-scale variability found in the individual anomaly fields (not shown), as well as in the derived statistics (Figs. 8 & 13), tended to get smoothed out.

As already discussed, the deviations found might also have been caused by inhomogeneities or other data problems at the individual stations (see Section 4.2). Furthermore, they could also be due to real

signals which were not correctly reproduced by the interpolation procedure, e.g. due to insufficient station density or the omission of relevant physiographic factors (see Section 4.3). A further possible error source could be the presence of purely local climate forcings, related, for instance, to urbanization or changes in land use. Pielke et al. (2002) also found substantial, difficult to explain, small-scale variability in temperature trends in an other mid-latitude region (Colorado, USA).

The causes of the small-scale variations not resolved by the gridded anomaly fields should be investigated further. Meanwhile, it is suggested that users of the data set either should use areal averages that are computed from a larger number of gridpoints (see Section 4.1), or, if they wish to use data from individual gridpoints, should also consider the associated error estimates (Figs. 4, 5, 10 & 11), for instance in the context of sensitivity analyses.

5. CONCLUSIONS

The constructed 50 yr data set enables analyses of the joint space-time variability of the Swiss temperature and precipitation fields at a relatively high spatial and temporal resolution.

The accuracy of the provided point estimates at the gridpoint locations varies strongly as a function of the interpolated variable, geographical location, and time of year. Detailed error statistics are available for comparison with alternative data sets and for sensitivity analyses by potential users.

The newly proposed interpolation method is superior to simple elevation-detrended interpolation with regard to long-term mean precipitation. It also proved superior to the IDW method for the interpolation of autumn and wintertime temperature anomalies, but otherwise in its present configuration it is worse than IDW for the interpolation of anomaly fields.

The estimated biases of the interpolations for most variables and regions are close to zero, indicating that areal averages from a large number of gridpoints are accurately reproduced. This suggests utility of the data set for the validation of climate models, the calculation of the water balance over larger areas, and the accuracy assessment of coarser gridded data sets.

The spatial patterns of the long-term mean fields, as well as the temporal variability of the anomaly fields are generally captured well by the interpolations. Larger systematic errors and error variances occur, however, at locations above ~2000 masl and in data-sparse areas in south-southeast Switzerland.

The measured climate anomalies and trends show substantial small-scale spatial variability, which is not well reproduced. The point estimates provided by the interpolations should therefore be interpreted with care.

LITERATURE CITED

Agnew MD, Palutikof JP (2000) GIS-based construction of baseline climatologies for the Mediterranean using terrain variables. Clim Res 14:115–127

Aschwanden A, Beck M, Häberli Ch, Haller G, Kiene M, Roesch A, Sie R, Stutz M (1996) Bereinigte Zeitreihen—die Ergebnisse des Projekts KLIMA90. Klimatologie der Schweiz (1961–1990), Heft 2, Band 1. Schweizerische Meteorologische Anstalt, Zurich

Bär H (1989) Kartographische Darstellungen von Wetter- und Klimadaten. Diploma thesis, Geographical Institute, University of Zurich

Barros AP, Lettenmaier DP (1994) Dynamic modelling of orographically induced precipitation. Rev Geophys 32:265–284

Basist A, Bell GD, Meentemeyer V (1994) Statistical relationships between topography and precipitation patterns. J Clim 7:1305–1315

Benichou P, Le Breton O (1987) Prise en compte de la topographie pour la cartographie des champs pluviométriques statistiques. La Météorologie 7:23–34

Böhm R, Auer I, Brunetti M, Maugeri M, Nanni T, Schöner W (2001) Regional temperature variability in the European Alps: 1760–1998 from homogenized instrumental time series. Int J Climatol 21:1779–1801

Brunsdon C, McClatchey J, Unwin DJ (2001) Spatial variations in the average rainfall-altitude relationship in Great Britain: an approach using geographically weighted regression. Int J Climatol 21:455–466

Carrega P (1995) A method for the reconstruction of mountain air temperatures with automatic cartographic applications. Theor Appl Climatol 52:69–84

Courault D, Monestiez P (1999) Spatial interpolation of air temperature according to atmospheric circulation patterns in southeast France. Int J Climatol 19:365–370

Daly C, Neilson RP, Phillips DL (1994) A statistical-topographic model for mapping climatological precipitation over mountainous terrain. J Appl Meteorol 33:140–158

Dodson R, Marks D (1997) Daily air temperature interpolated at high spatial resolution over a large mountainous terrain. Clim Res 8:1–20

Drogue G, Humbert J, Deraisme J, Mahr N, Freslon N (2002) A statistical-topographic model using an omnidirectional parameterization of the relief for mapping orographic rainfall. Int J Climatol 22:599–613

Frei C, Schär C (1998) A precipitation climatology of the Alps from high-resolution rain-gauge observations. Int J Climatol 18:873–900

Gyalistras D, Schär C, Davies HC, Wanner H (1998) Future Alpine climate. In: Cebon P, Dahinden U, Davies HC, Imboden D, Jäger CG (eds) Views from the Alps: re-

gional perspectives on climate change. MIT Press, Boston, p 171–223

Hastings DA, Dunbar PK (1998) Development and assessment of the Global Land One-km Base Elevation Digital Elevation Model (GLOBE). Int Soc Photgram Remote Sensing (ISPRS) Arch 32:218–221

Hirsch RM (1982) A comparison of four streamflow record extension techniques. Water Resour Res 18:1081–1088

Holdaway M (1996) Spatial modeling and interpolation of monthly temperature using kriging. Clim Res 6:215–225

Humbert J, Perron L, Perrin JL (1997) Precipitation mapping in mountainous area: comparison of two statistical models. In: Molnár L, Miklánek P, Mészáros I (eds) Developments in hydrology of mountainous areas. Proceedings Stara Lesna Conference, 12–16 September 1994, High Tatras, Slovakia. Technical Documents in Hydrology No. 8, UNESCO, Paris, p 70–75

Hutchinson MF (1995) Interpolating mean rainfall using thin plate smoothing splines. Int J Geogr Inf Syst 9:385–403

Hutchinson MF, Bischof RJ (1983) A new method for estimating the spatial distribution of mean seasonal and annual rainfall applied to the Hunter Valley, New South Wales. Aust Meteorol Mag 31:179–184

Kaplan A, Kushnir Y, Cane MA, Blumenthal MB (1997) Reduced space optimal analysis for historical data sets: 136 years of Atlantic sea surface temperatures. J Geophys Res 102:27835–27860

Kirchhofer W, Sevruk B (1992) Mittlere jährliche korrigierte Niederschlagshöhen 1951–1980. In: Spreafico M, Weingartner R, Leibundgut C (eds) Hydrological atlas of Switzerland. Landeshydrologie und -geologie, Bern, Plate 22

Kurtzman D, Kadmon R (1999) Mapping of temperature variables in Israel: a comparison of different interpolation methods. Clim Res 13:33–43

Landestopographie (2001a) DHM 25—das digitale Höhenmodell der Schweiz, Level 2. Technical Report, Swiss Federal Office of Topography, Wabern

Landestopographie (2001b) Formeln und Konstanten für die Berechnung der Schweizerischen schiefachsigen Zylinderprojektion und der Transformation zwischen Koordinatensystemen. Technical Report, Swiss Federal Office of Topography, Wabern

Leemans R, Cramer WP (1991) The IIASA database for mean monthly values of temperature, precipitation and cloudiness of a global terrestrial grid. Report No. RR-91-018, International Institute for Applied Systems Analysis (IIASA), Laxenburg

Menzel L (1999) Flächenhafte Modellierung der Evapotranspiration mit TRAIN. PIK Report No. 64, Potsdam Institute for Climate Impact Research, Potsdam

Menzel L, Lang H, Rohmann M (1999) Mittlere jährliche aktuelle Verdunstungshöhen 1973–1992. In: Spreafico M, Weingartner R, Leibundgut C (eds) Hydrological atlas of Switzerland. Landeshydrologie und -geologie, Bern, Plate 41

Neidhöfer F (2000) Interpolation and downscaling of precipitation in the Alps. PhD thesis, Institute of Geography, University of Bern

New M, Hulme M, Jones P (1999) Representing twentieth century space-time climate variability. Part I: Development of a 1961–90 mean monthly terrestrial climatology. J Clim 12:829–856

New M, Hulme M, Jones P (2000) Representing twentieth-century space-time climate variability. Part II: Development of 1901–96 monthly grids of terrestrial surface climate. J Clim 13:2217–2238

New M, Lister D, Hulme M, Makin I (2002) A high-resolution data set of surface climate over global land areas. Clim Res 21:1–25

Ninyerola M, Pons X, Roure JM (2000) A methodological approach of climatological modelling of air temperature and precipitation through GIS techniques. Int J Climatol 20:1823–1841

Pardo-Iguzquiza E (1998) Comparison of geostatistical methods for estimating the areal average climatological rainfall mean using data on precipitation and topography. Int J Climatol 18:1031–1047

Pepin N (2001) Lapse rate changes in northern England. Theor Appl Climatol 68:1–16

Phillips DL, Dolph J, Marks D (1992) A comparison of geostatistical procedures for spatial analysis of precipitation in mountainous terrain. Agric For Meteorol 58:119–141

Pielke RA Sr, Stohlgren T, Schell L, Parton W and 5 others (2002) Problems in evaluating regional and local trends in temperature: an example from eastern Colorado, USA. Int J Climatol 22:421–434

Preisendorfer RW (1988) Principal component analysis in meteorology and oceanography. Elsevier, Amsterdam

Prudhomme C, Reed DW (1998) Relationships between extreme daily precipitation and topography in a mountainous region: a case study in Scotland. Int J Climatol 18: 1439–1454

Purves RS, Hulton NRJ (2000) A climatic-scale precipitation model compared with the UKCIP baseline climate. Int J Climatol 20:1809–1821

Schär C, Davies T, Frei C, Wanner H, Widmann M, Wild M, Davies HC (1998) Current Alpine climate. In: Cebon P, Dahinden U, Davies HC, Imboden D, Jäger CG (eds) Views from the Alps: regional perspectives on climate change. MIT Press, Boston, p 21–72

Schmidli J, Frei C, Schär C (2001) Reconstruction of mesoscale precipitation fields from sparse observations in complex terrain. J Clim 14:3289–3306

Schmidli J, Schmutz C, Frei C, Wanner H, Schär C (2002) Mesoscale precipitation variability in the region of the European Alps during the 20th century. Int J Climatol 22: 1049–1074

Schmutz C (2001) Low frequency climate and precipitation variability in the Alpine region. PhD thesis, Institute of Geography, University of Bern

Schüepp M, Schirmer H (1977) Climates of central Europe. In: Wallén CC (ed) Climates of central and southern Europe. World survey of climatology. Elsevier, Amsterdam, p 3–74

Schüepp M, Bouët M, Bider M, Urfer C (1978) Regionale Klimabeschreibungen, 1. Teil. Beiheft zu den Annalen der Schweizerischen Meteorologischen Anstalt No. 18, Zurich

Schulla J (1997) Hydrologische Modellierung von Flussgebieten zur Abschätzung der Folgen von Klimaänderungen. PhD thesis No 12018, Swiss Federal Institute of Technology (ETH), Zurich [also available as Zürcher Geographische Schriften No. 69 (1997) Geographisches Institut, ETH, Zurich]

Schwarb M (2001) The Alpine precipitation climate. Evaluation of a high-resolution analysis scheme using comprehensive rain-gauge data. PhD thesis No. 13911, Swiss Federal Institute of Technology (ETH), Zurich [also available as Zürcher Klima-Schriften No. 80 (2001) Institute for Climate Research, ETH, Zurich]

Schwarb M, Frei C, Daly C, Schär C (2001) Mean seasonal precipitation throughout the European Alps 1971–1990. In: Spreafico M, Weingartner R, Leibundgut C (eds) Hydrological atlas of Switzerland. Landeshydrologie und geologie, Bern, Plate 27

Sevruk B (1985) Systematischer Niederschlagsmessfehler in

der Schweiz. In: Sevruk B (ed) Der Niederschlag in der Schweiz. Beitr Geol Schweiz Hydrol 31:65–75

Shepard DS (1984) Computer mapping: the SYMAP interpolation algorithm. In: Gaile GL, Willmott CJ (eds) Spatial statistics and models. Reidel, Dordrecht, p 133–145

Thompson CS, Sinclair MR, Gray WR (1997) Estimating long-term annual precipitation in a mountainous region from a diagnostic model. Int J Climatol 17:997–1007

Vogt JV, Viau AA, Paquet F (1997) Mapping regional air temperature fields using satellite-derived surface skin temperatures. Int J Climatol 17:1559–1580

Wanner H, Gyalistras D, Luterbacher J, Rickli R, Salvisberg E, Schmutz C (2000) Klimawandel im Schweizer Alpenraum. Hochschulverlag, Swiss Federal Institute of Technology (ETH), Zürich

Willmott CJ, Rowe CM, Philpot WD (1985) Small-scale climate maps: a sensitivity analysis of some common assumptions associated with grid-point interpolation and contouring. Am Cartogr 12:5–16

Zevenbergen LW, Thorne CR (1987) Quantitative analysis of land surface topography. Earth Surf Process Landform 12:47–56

Z'graggen L (2001) Strahlungsbilanz der Schweiz. PhD thesis No. 14158, Swiss Federal Institute of Technology (ETH), Zurich

Zheng X, Basher RE (1996) Spatial modelling of New Zealand temperature normals. Int J Climatol 16:307–320

Zierl B (2000) WAWAHAMO—a hydrological model to simulate drought in forested ecosystems. PhD thesis No. 1320, University of Fribourg and Swiss Federal Institute for Forest, Snow and Landscape Research (WSL), Birmensdorf

Zierl B (2001) A water balance model to simulate drought in forested ecosystems and its application on the entire forested area of Switzerland. J Hydrol 242:115–136